

Layer codes

Dominic J. Williamson¹ and Nouédyn Baspin¹

¹*Centre for Engineered Quantum Systems, School of Physics,
University of Sydney, Sydney, NSW 2006, Australia*

(Dated: May 2023)

The surface code is a two dimensional topological code with code parameters that scale optimally with the number of physical qubits, under the constraint of two dimensional locality. In three spatial dimensions an analogous simple yet optimal code was not previously known. Here, we introduce a construction that takes as input a stabilizer code and produces as output a three dimensional topological code with related code parameters. The output codes have the special structure of being topological defect networks formed by layers of surface code joined along one dimensional junctions, with a maximum stabilizer check weight of six. When the input is a family of good low density parity check codes, the output is a three dimensional topological code with optimal scaling code parameters and a polynomial energy barrier.

CONTENTS

I. Introduction	2
II. Background	10
III. Layer Code Construction	16
IV. Code Properties	32
V. Proof of Main Results	38
VI. Lattice Model	44
VII. Discussion	55
References	57

I. INTRODUCTION

Quantum computing promises to open a new window into highly-entangled quantum many-body physics [1–5]. Quantum error correction is a crucial ingredient in the design of scalable quantum computers that aim to access new regimes of physics beyond the reach of classical simulations [6–14]. Topological quantum codes form the basis of leading approaches to implement quantum error correction [15–22]. This can be attributed to their favourable properties, including relatively simple stabilizer checks and high thresholds. Topological codes form an important subclass of low density parity check (LDPC) codes [23–26], set apart by the geometric locality of their checks.

The surface code is the simplest example of a topological code and as such is the most widely studied quantum error-correcting code both theoretically and experimentally [15–22]. It is known by several names including the toric code, the planar code, \mathbb{Z}_2 lattice gauge theory, the \mathbb{Z}_2 quantum double, and $\mathcal{Z}(\text{Vec}_{\mathbb{Z}_2})$ [15, 16, 27–30]. Despite its popularity and positive features, the surface code is far from attaining optimal scaling of its code parameters $[[n, k, d]]$. Here n is the number of physical qubits, k is the number of encoded qubits, and d is the code distance, i.e. the minimum weight of a nontrivial logical operator. The surface code is a $[[2L(L-1), 1, L]]$ code and hence has a vanishing rate $\frac{k}{n}$ and suboptimal distance scaling when compared to general LDPC stabilizer codes which can achieve a constant $\frac{d}{n}$ scaling. In a recent flurry of work, *good* LDPC codes were discovered [31–36] that attain code parameters with optimal scaling i.e. $[[n, \Theta(n), \Theta(n)]]$.

Topological codes defined on a regular lattice in D -dimensional Euclidean (flat) space with a finite density of qudits can never attain optimal scaling of the code parameters. This is because they are constrained by several bounds, including the Bravyi-Poulin-Terhal (BPT) bound [37]

$$kd^{\frac{2}{D-1}} \leq O(n), \quad (1)$$

the Bravyi-Terhal (BT) bound [38]

$$d \leq O(n^{\frac{D-1}{D}}), \quad (2)$$

and Haah's bound [39]

$$k \leq O(n^{\frac{D-2}{D}}). \quad (3)$$

In light of these bounds, the best scaling of code parameters for a topological code in D dimensions one can hope to achieve is $[[n, \Theta(n^{\frac{D-2}{D}}), \Theta(n^{\frac{D-1}{D}})]]$. Writing these code parameters in terms of the linear extent of a hypercuboid lattice L we find $[[\Theta(L^D), \Theta(L^{D-2}), \Theta(L^{D-1})]]$. The most physically

relevant cases are $D = 2, 3$. It is apparent from the parameters given above that the surface code achieves optimal scaling for $D = 2$. Here, we introduce families of *layer codes* that achieve optimal scaling for $D = 3$.

A. Overview of Main Results

In this work we introduce a construction that takes as input an arbitrary Calderbank-Shor-Steane [40, 41] (CSS) stabilizer code and outputs a topological CSS code that is local in dimension $D = 3$ which we call a *layer code*. The code parameters of the input and output codes of our construction are related by

$$[[n, k, d]] \mapsto [[\Theta(nn_X n_Z), k, \Omega(\frac{d}{w} n_*)]], \quad (4)$$

where n_X is the number of X checks, n_Z is the number of Z checks, $n_* = \min(n_X, n_Z)$, and w is the maximum weight of the checks in the input code. Furthermore, the maximum check weight of the output code is 6.

The layer codes output by our construction have additional structure, taking the form of topological defect networks [42–44]. More specifically, each layer code is constructed from layers of surface code with one layer for each physical qubit, X check, and Z check of the input code. The surface code layers associated to physical qubits are stacked on xz planes of a cubic lattice, the layers associated to X checks are stacked on xy planes, and the layers associated to Z checks are stacked on yz planes. The grid of surface code layers are then coupled together at nontrivial junctions that are determined by the Tanner graph of the input code.

When applied to a family of good CSS LDPC codes our construction outputs a family of topological CSS codes that achieve optimal scaling of the code parameters for $D = 3$, that is

$$[[n, \Theta(n), \Theta(n)]] \mapsto [[\Theta(n^3), \Theta(n), \Theta(n^2))]]. \quad (5)$$

We further demonstrate that our construction preserves the scaling of the energy barrier when the input code is LDPC. We show that a family of good CSS LDPC codes from Ref. [35] has energy barrier $\Theta(n)$. This leads to our main result

Theorem 1. *There exist families of topological CSS stabilizer codes in $D = 3$ spatial dimensions that achieve the optimal code parameters $[[\Theta(L^3), \Theta(L), \Theta(L^2)]]$ and a $\Theta(L)$ energy barrier. In particular, layer codes based on the good LDPC codes from Ref. [35] achieve these properties and have checks of weight 6 or less.*

Proof. In Section IV A we explain how the code parameters of the layer codes are related to those of the input codes. This is summarized in Eq. (4). In Section IV B we explain how the scaling of the energy barrier for a layer code is related to the energy barrier of the input code. In Section V A we present technical lemmas characterizing the form of the logical operators in the layer codes. We rely upon this characterization to establish the scaling of the distance, number of encoded qubits and energy barrier. In Section V B we show that the family of good CSS LDPC codes from Ref. [35] has energy barrier $\Theta(n)$. In Section VI we introduce a lattice model for the layer codes involving local stabilizer generators of weight at most 6. The results in Section IV applied to the codes from Ref. [35] results in families of layer codes with the claimed properties. \square

The layer code construction opens the door to a vast, unexplored landscape of promising non translation-invariant topological codes with striking features. Table I provides a summary of the input and output codes involved in the construction. Algorithm 1 provides a summary of the construction procedure.

Input code	Output layer code
General CSS stabilizer code	3D topological defect network code
Physical qubit	xz surface code layer
X check	xy surface code layer
Z check	yz surface code layer
Max check weight w	Max check weight 6
Energy barrier $\Delta(n)$	Energy barrier $\frac{1}{ww'}\Delta(n)$
$[[n, k, d]]$	$[[\Theta(nn_Xn_Z), k, \Omega(\frac{1}{w}d \min(n_X, n_Z))]]$

TABLE I. Summary of the input and output code properties in the layer code construction.

B. Prior Work

Quantum codes in three dimensions have received a significant amount of attention over the past two decades [17, 45–69]. A stack of L two dimensional surface codes of size $L \times L$ demonstrates the possibility of three dimensional topological codes with a number of encoded qubits that scales as $\Theta(L)$. The three dimensional toric code [17] established that planelike logical operators with minimum weight $\Omega(L^2)$ are possible in three dimensional topological codes. However the distance of the three dimensional toric code scales as $\Theta(L)$ as it also supports a stringlike logical operator. This further implies that the three dimensional toric code has a constant logical energy barrier and

hence is not a self-correcting quantum memory [48, 49]. There have been numerous efforts searching for codes beyond the toric code which have no stringlike logical operators and consequently have superlinear distances and logical energy barriers that increase with system size. Research in this area has resulted in the discovery of a number of fracton codes [52, 53, 55–58]. One particularly remarkable fracton code is Haah’s cubic code which has no stringlike logical operators, a superlinear distance, a logarithmic energy barrier, a number of encoded qubits that scales as $\Theta(L)$ for a family of system sizes, and which exhibits partial self correction [53, 62, 63]. The cubic code, and other so-called type-II fracton models that satisfy the no stringlike logical operator rule, have superlinear distances and a number of encoded qubits that scales as $\Theta(L)$ for certain sequences of system sizes, yet none has been shown to achieve optimal $\Theta(L^2)$ scaling of the code distance. Codes with polynomially growing energy barriers have been found by abandoning translation invariance [61]. However, these codes also failed to achieve optimal scaling of the code distance. The layer codes output by our construction can be viewed as a new variety of non translation invariant fracton codes which can achieve the desired optimal code parameters $[\Theta(L^3), \Theta(L^1), \Theta(L^2)]$ and a logical energy barrier that scales as $\Theta(L)$.

A large amount of research has been done on new constructions of fracton models and attempts to characterize and classify them [57–59, 70–87]. This led to the discovery that networks of two and three dimensional topological codes joined together by topological defects can recover all known fracton models (with finite order excitations) [43, 44]. The layer codes introduced in this work are local topological codes in three spatial dimensions that take the form of topological defect networks. However, unlike previous topological defect network constructions, they are not translation invariant even at a coarse grained scale. The construction of layer code topological defect networks in this work is different to the topological defect network code construction introduced in Ref. [44]. For contrast, the earlier construction takes as input a topological CSS code that is already local in a fixed spatial dimension, and produces as output a new topological CSS code that is local in the same spatial dimension but has the special form of a topological defect network. The layer codes in this work are also related to the gauged layer constructions in Refs. [86, 87]. The models in both the present and previous works can be understood as resulting from gauging planar symmetries formed by the product of stringlike logical operators over layers of surface code stacked along one direction. However in the previous works the products were taken over all layers, whereas in this work the layers involved in each product are determined by the checks of an input CSS code.

Note added — While this project was in progress [88], a manuscript proving a related result appeared [89] which also builds upon the recent breakthroughs establishing good LDPC codes [26, 34–

[36] to construct new topological codes in $D \geq 3$. Our construction was formulated and worked out independently of Ref. [89] and differs on several key points. First, our work makes no use of the main techniques employed in Ref. [89], including the construction due to Freedman and Hastings [90] and a quantitative embedding theorem due to Gromov and Guth [91]. The distinction is further accentuated by the special structure inherent to the layer codes output by our construction, they are topological defect networks made up of surface code layers and defects with maximum check weight 6, which does not appear to hold for the codes in Ref. [89]. Finally, we remark that while our construction is only defined for $D = 3$ it saturates the BPT bound without any polylog factor, whereas the result in Ref. [89] applies to arbitrary finite D but only achieves optimal code parameter scaling up to a polylog factor. The precise relationship between the construction we present here and that of Ref. [89] is an interesting question we leave to future work.

C. Examples

We now illustrate our construction by depicting the layer codes that are output given several simple examples of input CSS codes.

1. Repetition Code

The first example is based on the 3 qubit repetition code, which has stabilizer checks ZZI, IZZ . The layer code derived from the 3 qubit repetition code involves 5 surface code layers in total. There are 3 xz surface code layers corresponding to the input physical qubits, and 2 yz surface code layers corresponding to the input code Z checks. Trijunction topological defects join the check layers to the qubit layers as shown in Figure 1 below, the details of these defects are explained in Section III.

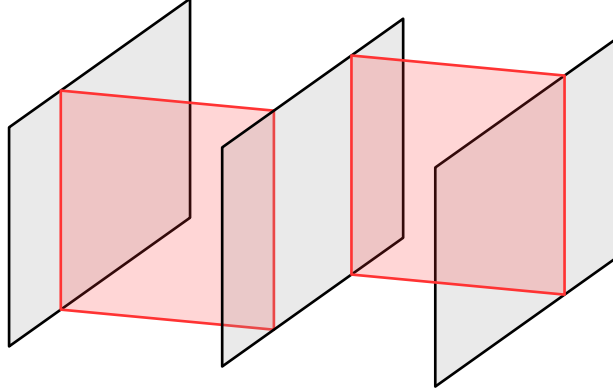


FIG. 1. The layer code based on the 3 qubit repetition code. 3 grey xz layers depict surface codes corresponding to input physical qubits. 2 red yz layers depict surface codes corresponding to input Z checks. Trijunctions between the red and grey layers correspond to nontrivial topological defects.

2. $[[4,2,2]]$ error detecting code

The $[[4,2,2]]$ error detecting code has the following stabilizer checks $XXXX, ZZZZ$. The layer code based on the $[[4,2,2]]$ code involves 6 surface code layers in total, 4 xz layers corresponding to encoded qubits, 1 xy layer corresponding to the X check, and 1 yz layer corresponding to the Z check. The surface code layers are joined together at their junctions by topological defects as shown in Figure 2, see Section III for a detailed description of the defects.

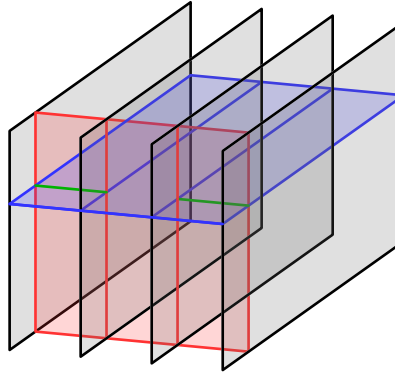


FIG. 2. The layer code based on the $[[4,2,2]]$ code. 4 grey xz layers depict surface codes corresponding to input physical qubits. The blue xy layer depicts a surface code corresponding to an input X check. The red yz layer depicts a surface code corresponding to an input Z check. Blue, red and green junctions where the layers meet correspond to nontrivial topological defects.

3. Shor's Code

Shor's code has the following stabilizer checks [6]

$$\begin{aligned}
 & X \ X \ X \ X \ X \ X \ I \ I \ I \\
 & I \ I \ I \ X \ X \ X \ X \ X \ X \\
 & Z \ Z \ I \ I \ I \ I \ I \ I \ I \\
 & I \ Z \ Z \ I \ I \ I \ I \ I \ I \\
 & I \ I \ I \ Z \ Z \ I \ I \ I \ I \\
 & I \ I \ I \ I \ Z \ Z \ I \ I \ I \\
 & I \ I \ I \ I \ I \ I \ Z \ Z \ I \\
 & I \ I \ I \ I \ I \ I \ I \ Z \ Z.
 \end{aligned} \tag{6}$$

The layer code based on Shor's code involves 17 surface code layers in total, 9 xz layers corresponding to encoded qubits, 2 xy layers corresponding to X checks, and 6 yz layers corresponding to Z checks. These surface code layers are joined together at their junctions by defects that follow the incidence relations of the qubits and checks in Shor's code, see Figure 3. The defects are described in Section III.

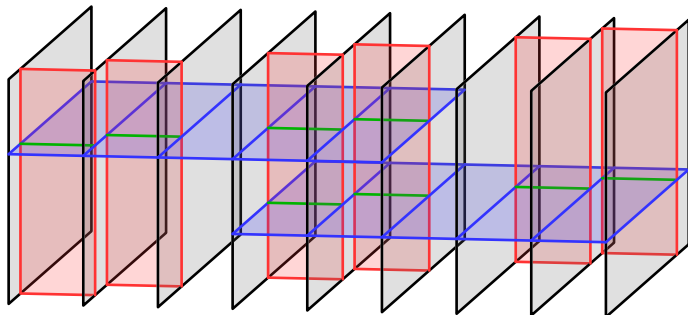


FIG. 3. The layer code based on Shor's code. 9 grey xz layers depict surface codes corresponding to input physical qubits. 2 blue xy layers depict surface codes corresponding to input X checks. 6 red yz layers depict surface codes corresponding to input Z checks. Blue, red and green junction lines where the layers meet correspond to nontrivial topological defects.

4. Steane's Code

Steane's code has the following stabilizer checks [92]

$$\begin{array}{cccccccc}
 X & I & X & I & X & I & X \\
 I & X & X & I & I & X & X \\
 I & I & I & X & X & X & X \\
 Z & I & Z & I & Z & I & Z \\
 I & Z & Z & I & I & Z & Z \\
 I & I & I & Z & Z & Z & Z.
 \end{array} \tag{7}$$

The layer code based on Steane's code involves 13 surface code layers in total, 7 xy layers corresponding to encoded qubits, 3 xy layers corresponding to X checks, and 3 yz layers corresponding to Z checks. The surface code layers are joined together at their junctions by topological defects as described in Section III. The resulting layer code is depicted in Figure 4

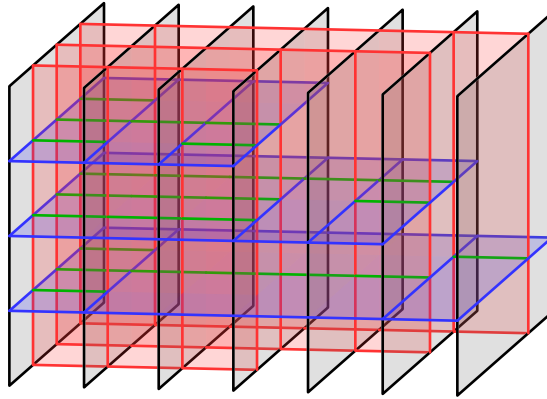


FIG. 4. The layer code based on Steane's code. 7 grey xz layers depict surface codes corresponding to input physical qubits. 3 blue xy layers depict surface codes corresponding to input X checks. 3 red yz layers depict surface codes corresponding to input Z checks. Blue, red and green junction lines where the layers meet correspond to nontrivial topological defects.

D. Section Outline

In Section II we review relevant background material. In Section III we explain the layer code construction. In Section IV we describe the properties of the layer codes. In Section V we provide proofs of our main results. In Section VI we describe explicit stabilizer checks to implement layer codes on the lattice. In Section VII we discuss our results and future directions.

II. BACKGROUND

In this section we summarize relevant background material that we build upon in the layer code construction.

A. Quantum Codes

A n -qubit quantum code \mathcal{C} is a subset of a n -qubit Hilbert space $(\mathbb{C}^2)^{\otimes n}$. We say that \mathcal{C} encodes k logical qubits if $\mathcal{C} \cong (\mathbb{C}^2)^{\otimes k}$. In this work we will focus on stabilizer codes, where \mathcal{C} is the common $+1$ eigenspace of \mathcal{S} , an abelian subgroup of the n -qubit Pauli group. Further, a code is CSS if $\mathcal{S} = \mathcal{S}_X \cdot \mathcal{S}_Z$, where \mathcal{S}_X and \mathcal{S}_Z are generated, respectively, by X -type and Z -type Pauli operators. Finally, the distance d of a stabilizer code is the support of the smallest operator L such that L commutes with all elements in \mathcal{S} yet is not in \mathcal{S} .

B. Surface Code

The surface code refers to a family of $n = \Theta(L_x \times L_z)$ qubit CSS stabilizer codes [12]. The qubits are associated to edges of an $L_x \times L_z$ patch of the square lattice with two *smooth* boundaries at $x = 0, L_x$ and two *rough* boundaries at $z = 0, L_z$, see Fig. 5. The stabilizer group is generated by star and plaquette checks

$$\mathcal{S} = \langle A_v, B_p \mid A_v = \prod_{v \ni e} X_e, B_p = \prod_{e \in p} Z_p \rangle. \quad (8)$$

The stabilizer checks in the bulk have weight 4, while the boundary stabilizer checks have weight 3. Note vertices along the smooth boundary, and plaquettes along the rough boundary are included in the patch of square lattice. Counting the number of qubits and independent stabilizer checks reveals there is a single encoded qubit. Logical representatives are given by a horizontal X string operator and a vertical Z string operator

$$\overline{X} = \prod_{e \in \hat{\gamma}_x} X_e, \quad \overline{Z} = \prod_{e \in \gamma_z} Z_e, \quad (9)$$

where $\hat{\gamma}_x$ is a path through the dual lattice running from $x = 0$ to $x = L_x$, and γ_z is a path through the lattice running from $z = 0$ to $z = L_z$.

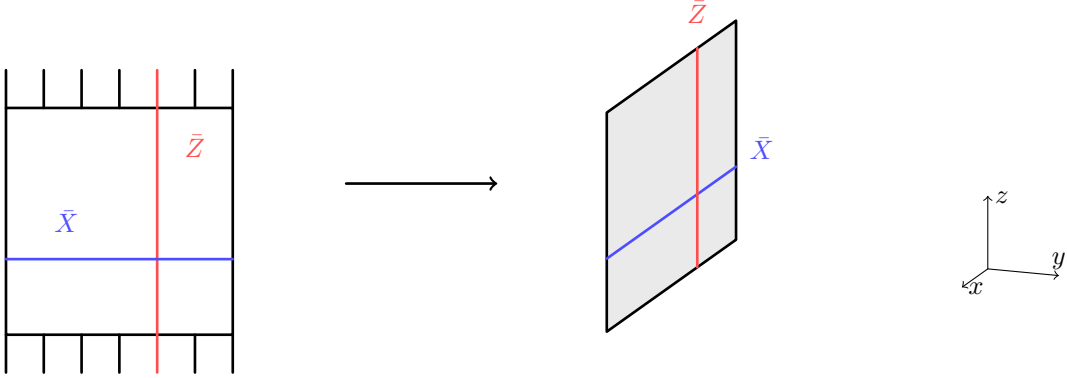


FIG. 5. On the left is the usual representation of the surface code with rough and smooth boundaries such that the \bar{Z} logical operator runs from top to bottom, while the \bar{X} logical operator runs from left to right. Throughout the rest of this section we represent the surface code in 3D space with the same boundary conditions oriented such that the \bar{Z} operator runs along the \hat{z} axis, and the \bar{X} operator runs along the \hat{x} axis. In the three dimensional picture the rough boundaries are left implicit.

1. Anyons and Superselection Sectors

The surface code can be formulated as the ground space of a local Hamiltonian in two dimensions

$$H = - \sum_v A_v - \sum_p B_p. \quad (10)$$

The surface code Hamiltonian has an energy gap, and lies in a nontrivial quantum phase of matter [93], meaning it cannot be connected to a trivial decoupled Hamiltonian via a gap preserving continuous adiabatic deformation as $L_x, L_z \rightarrow \infty$. This phase of matter has a property known as topological order, which requires that the projection of any local operator onto the degenerate ground space is proportional to the identity [94]. This is similar to the Knill-Laflamme condition for the detection and correction of local errors [95]. While all local operators act trivially within the ground space, local excitations can be nontrivial. These local excitations correspond to syndromes of the surface code, i.e. collections of stabilizer generators with eigenvalue -1 , within a local region of the lattice. Following Ref. [15] we call an $A_v = -1$ syndrome an e anyon, which can be created by a Z string operator, while we call a $B_p = -1$ syndrome an m anyon, which can be created by an X string operator.

Local excitations in the surface code are organized into equivalence classes known as *superselection sectors* [30]. A pair of local excitations E_1, E_2 , is considered equivalent if E_1 can be converted to E_2 via the application of a local operator, and vice versa. In the surface code there are four superselection sectors known as the vacuum, electric charge, magnetic flux, and dyon, which we

label $\{1, e, m, \psi\}$ respectively, where $\psi = e \times m$. Since e and m anyons are always created in pairs by local operators contained within the bulk of the surface code, the trivial sector 1 corresponds to an even number of both e and m anyons. The superselection sector e collects all excitations with an odd number of e anyons, while m is the sector corresponding to an odd number of m anyons. A pair of superselection sectors can be *fused* by considering representative local excitations for each on adjacent regions A and B and then taking equivalence classes under local operators on a larger region C that contains both A and B . The *fusion* rules of the surface code superselection sectors are given by \mathbb{Z}_2^2 . A pair of superselection sectors can also be *braided* by moving one around the other using string operators. The nontrivial braiding properties of the surface code anyons are generated by a -1 braiding process between e and m due to the anticommutation of the relevant X and Z string operators. The braiding statistics of abelian anyons, such as those of the surface code, can be extracted from the *exchange* statistics of the particles. It is possible to extract these from the lattice following the procedure in Refs. [96, 97]. In the surface code, the only nontrivial exchange statistic is a -1 associated to the emergent fermion ψ . The fusion and braiding structure for the surface code anyons is represented abstractly by a modular tensor category [30, 98] that is denoted $\mathcal{Z}(\text{Vec}_{\mathbb{Z}_2})$.

2. Boundaries, Defects and Condensation

Boundaries of the surface code are determined by the condensation of anyons [99–103]. For our purposes, anyon condensation in a topological phase refers to the identification of otherwise distinct superselection sectors near a topological *defect*. A defect is a modified region of a topological code or Hamiltonian where different stabilizers or Hamiltonian terms are introduced. Examples of defects are given by the rough and smooth boundaries in the surface code. A defect is *topological* if its properties, such as which anyons condense there, do not depend on the microscopic realization of the defect such as its precise shape. In this sense it is often said that topological defects are deformable. A defect is said to be *gapped* if the topological order condition is still satisfied after the defect is introduced. An anyon is said to *condense* on a defect if it can be created by a local operator on a region containing the defect. We remark that in the absence of a defect, anyons in nontrivial superselection sectors cannot be created by local operators. However, in the vicinity of a defect the trivialization of anyons in nontrivial superselection sectors becomes possible. That is, near a defect some anyons that would otherwise be nontrivial can be created or annihilated by the application of local operators, see Figure 6. Anyon condensation must satisfy certain consistency

conditions [101, 103]. In an abelian anyon theory such as the surface code the condensing anyons form a subgroup of all anyons under fusion [102].

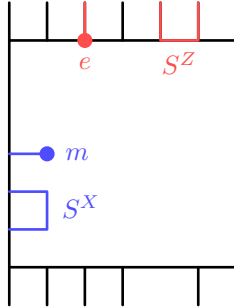


FIG. 6. Operators and anyons condensing at the rough and smooth boundary of surface code.

Topological line defects are a ubiquitous class of defects that appear throughout this work. A fundamental type of line defect is known as a gapped boundary [99, 100]. At a gapped boundary there are additional consistency constraints on the anyons that can condense there [101–103]. The anyons that condense at a gapped boundary must braid trivially with one another, and each anyon must have trivial exchange statistics¹. Furthermore, the algebra of condensing anyons must be maximal meaning all anyons that do not condense braid nontrivially with some anyon that does condense. Intuitively, this condition ensures that the condensation of anyons at the boundary leaves nothing behind, and hence is consistent with a gapped boundary with nothing on the other side. For abelian anyon theories these conditions are summarized by an object known as a Lagrangian subgroup [102].

Lemma 1 ([102]). *There is a one-to-one mapping between Lagrangian subgroups of an abelian anyon theory and gapped boundaries.*

A general line defect in two dimensions can connect a pair of topological phases. This includes line defects formed by gapped boundaries for each topological phase that meet along the defect line placed next to one another. A range of other defects are also possible. If the topological phases meeting at a line defect are equivalent, i.e. they are described by the same anyon theory, the defect may be *invertible*. An invertible line defect is one that has an inverse, for example the electromagnetic duality line defect in surface code [105]. That is, composing the defect with its inverse defect results in a line defect that is trivial, i.e. does nothing to the anyons passing through it. The anyons that condense on an invertible line defect must come in pairs, consisting of an

¹ In the presence of physical fermions this condition is loosened to allow condensing anyons to have fermionic exchange statistics [104].

anyon on each side of the defect that are related by an isomorphism. Defects that factorize into gapped boundaries from either side are, in a sense, as far as possible from being invertible. That is, there is a maximal set of anyons on either side that can condense on the line defect. On the other hand, all line defects can be reinterpreted as gapped boundaries of some topological phase via the *folding trick* [100]. The folding trick maps an arbitrary line defect to a gapped boundary by folding along the defect line, thereby stacking the topological phases on either side of the line defect onto one another, see Figure 7.



FIG. 7. An illustration of the folding trick applied to a line defect (left) to produce an equivalent gapped boundary (right).

In this work we focus on line defects that reduce to gapped boundaries of multiple copies of the surface code under the folding trick. Gapped boundaries of several copies of the surface code are described by Lagrangian subgroups of surface code anyons. A Lagrangian subgroup for c copies of surface code is defined by a set of c independent nontrivial anyons with trivial self-statistics, and trivial mutual braiding statistics. For a single copy of surface code the possible choices of generator for a Lagrangian subgroup are e or m , which correspond to rough and smooth boundaries, respectively. The Lagrangian subgroup description of a line defect specifies the anyon types that can be locally created in the vicinity of the defect. This information can then be used to derive products of string operators near the defect that create pairs of anyons and push them into the defect, leaving behind no excitations [102]. Such operators are commonly referred to as condensed on the line defect. This picture can be used to derive stabilizer generators for the defect on the lattice. For example, a single copy of the surface code with a gapped boundary defined by the condensation of e has short e string operators that end on the gapped boundary. Converting these short strings into lattice operators produces the 3-body rough boundary B_p terms introduced in Eq. (8). A similar procedure applied to m condensing boundaries produces the smooth boundaries of the surface code, see Figure 6.

The layer code construction also involves point defects, where line defects meet in multiple copies of surface code. Point defects in a two dimensional topological phase are described by

projection operators in the *annulus algebra* that surrounds them. An annulus algebra is generated by equivalence classes of all operators supported on an annulus shaped region that create no excitations, modulo the subalgebra of operators that are local within a dislike subregion of the annulus and create no excitations [106]. For a stabilizer code this corresponds to the group of logical operators supported on an annulus, modulo stabilizers supported on dislike subregions of the annulus. Intuitively this separates the stringlike operators that wrap around the annulus from the short loops that do not. The annulus algebra is a matrix algebra, and can be decomposed into irreducible representation blocks. Each irreducible block corresponds to a definite type of point defect. The projection operator in the annulus algebra that picks out a certain block can be converted into stabilizer generators that realize the corresponding point defect on the lattice [106]. A special case of the annulus algebra for a single copy of surface code with no line defects reduces to a \mathbb{Z}_2^2 algebra of closed loop operators generated by e and m loops. The projection operators in this algebra pick out states which have ± 1 braiding statistics with e, m , respectively. These four sectors precisely specify the four anyon types due to the modularity, or nondegeneracy, of the braiding [30]. Converting the annulus projection operators into lattice operators generates the familiar star and plaquette stabilizer checks of the surface code.

C. Energy Barrier

In this subsection we introduce the energy barrier of a quantum stabilizer code.

The *energy penalty* of a Pauli operator is defined to be the weight of the syndrome generated by that operator. The energy barrier of a sequence of single qubit Pauli operators $(P_i)_{i=1}^N$ is the maximum energy penalty of their cumulative product $(\prod_{i=1}^j P_i)_{j=1}^N$. The energy barrier of a multi-qubit Pauli operator L is defined to be the minimum energy barrier over all sequences $(P_i)_{i=1}^N$ of single qubit Pauli operators such that $\prod_{i=1}^N P_i = L$. The energy barrier of a logical class is defined to be the minimum energy barrier for any logical representative in the logical class. The *energy barrier* of a code is the minimum energy barrier of a nontrivial logical class. The above definitions have variants that are restricted to products of Pauli X (or Z) operators. A more universal definition allows for a product of a constant number of Pauli operators to be applied at each step, rather than single Pauli operators. For LDPC codes, the scaling of the energy barrier with the total number of qubits under both the more and less restrictive definitions must match, up to a universal constant, since applying a constant number of Pauli operators at once can only change the energy penalty by a constant amount.

III. LAYER CODE CONSTRUCTION

In this section we describe the central construction of the current work. This construction takes as input an arbitrary CSS stabilizer code and produces as output a layer code. Layer codes are three dimensional topological CSS codes formed by stacks of surface codes, one for each physical qubit, X check, and Z check of the input code, joined together by topological defect lines in a pattern that is based on the Tanner graph of the input code.

The core idea behind the construction is fairly simple. Our goal is to find topological CSS codes in three dimensions that saturate the BPT bound. We start from the observation that concatenating an $[[n, \Theta(n), \Theta(n)]]$ good CSS quantum code \mathcal{C} with an $[[L^2, 1, \Theta(L)]]$ surface code \mathcal{C}_S produces an $[[nL^2, \Theta(n), \Theta(nL)]]$ code with very high stabilizer weight and long range interactions but whose code parameters saturate the BPT bound for $L = \Theta(n)$. Our goal is then to reduce the stabilizer weight and interaction range back to constant without sacrificing the desired code parameters.

Fortunately, lattice surgery [107] can address both of these issues. For example, a $\bar{Z}\bar{Z}$ check between two distant patches of surface code can be inferred via local stabilizer measurements using a surgery patch. One can then imagine replacing all the high-weight long-range checks with lattice surgery patches to obtain a 3D local code with parameters $[[\Theta(L^3), \Theta(L), \Theta(L^2)]]$.

This approach, however, quickly runs into issues, as surgery patches for X -type checks do not commute with those for Z -type checks when they act on the same qubit of \mathcal{C} , or equivalently, on the same surface code patch of the concatenated code. The final ingredients we introduce are topological defects that allows us to “sew together” lattice surgery patches that act on the same qubits, in a way that restores commutation and preserves the desired code parameters and locality properties.

A. Overview

Before explaining the details of the layer code construction, we present a high level overview in Algorithm 1. Figure 8 illustrates the steps of the algorithm when applied to Shor’s code as an input.

Algorithm 1 Layer code construction

Require: An LDPC CSS code \mathcal{C} , with parameters $[[n, k, d]]$, n_X X -type checks, n_Z Z -type checks, and maximum check weight w .

Ensure: A CSS code that is local in 3D with parameters $[[\Theta(nn_Xn_Z), k, \Omega(\frac{1}{w}d \min(n_X, n_Z))]]$.

for each qubit $i \in [0, \dots, n - 1]$ **do**

 Create an xz layer \mathcal{D}_i , with the boundary conditions specified in Figure 5. (Depicted in Figure 8 a).

end for

for each s_j in the Z -type checks of \mathcal{C} **do**

 Let i_1, \dots, i_T be the qubits in the support of s_j . Create a yz -layer \mathcal{Z}_j starting from \mathcal{D}_{i_1} , going through each of the \mathcal{D}_{i_t} until \mathcal{D}_{i_T} , with the specifications given in Section III E and illustrated in Figure 14. (Depicted in Figure 8 b).

end for

for each \tilde{s}_k in the X -type checks of \mathcal{C} **do**

 Let i_1, \dots, i_T be the qubits in the support of \tilde{s}_k . Create an xy -layer \mathcal{X}_k starting from \mathcal{D}_{i_1} , going through each of the \mathcal{D}_{i_t} until \mathcal{D}_{i_T} , with the specifications given in Section III E, and illustrated in Figure 15. (Depicted in Figure 8 c).

end for

for each s_j in the Z -type checks of \mathcal{C} **do**

for each \tilde{s}_k in the X -type checks of \mathcal{C} **do**

 If the support of s_j and \tilde{s}_k overlap, introduce line and point defects between the layers \mathcal{Z}_j and \mathcal{X}_k following the specifications of Section III F. (Depicted in Figure 8 d).

end for

end for

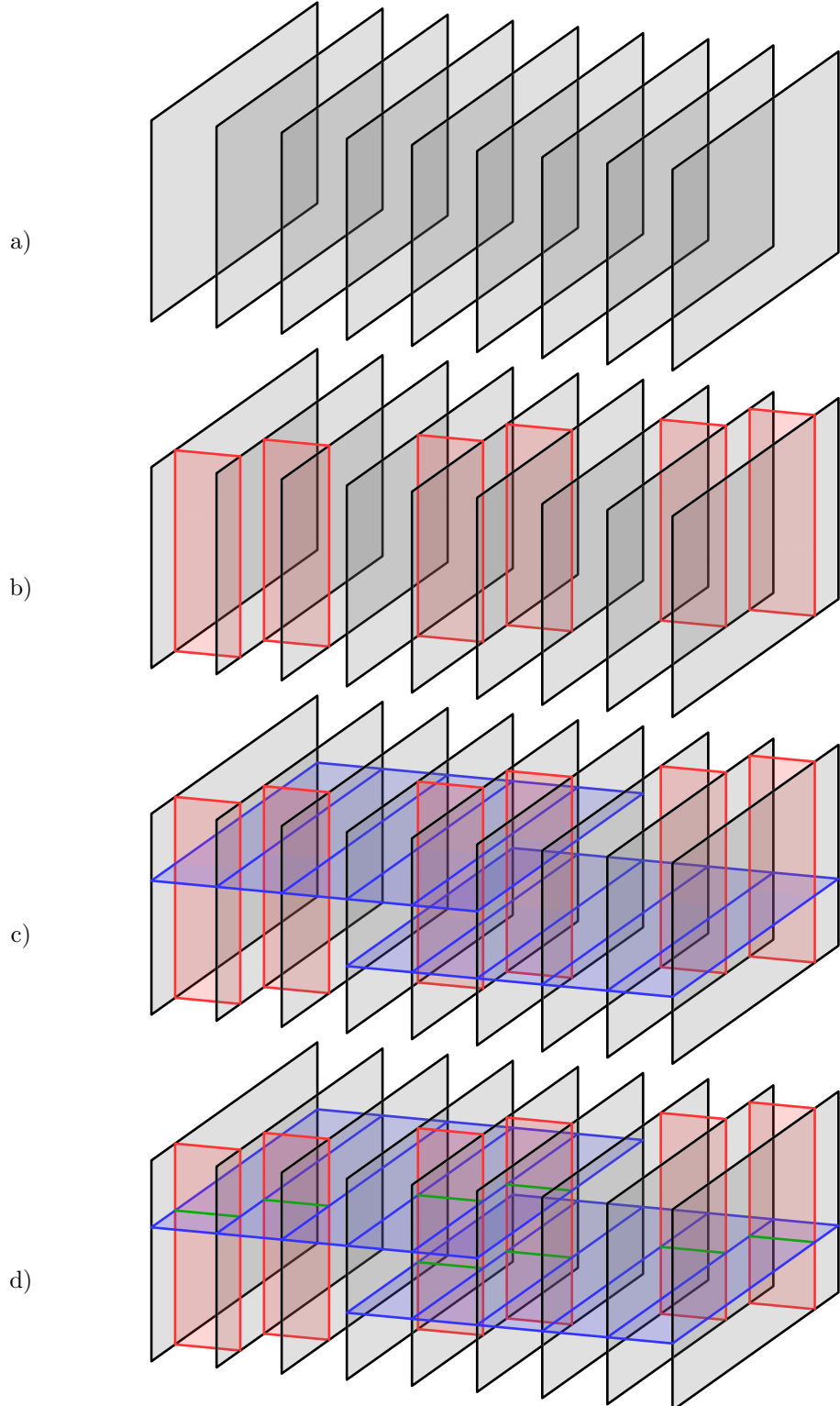


FIG. 8. Steps of the layer code construction outlined in Algorithm 1 when applied to Shor's code.

B. Lattice surgery as a topological defect.

We start by reviewing lattice surgery on the surface code from a topological quantum field theory [108, 109] (TQFT) lens. This allows us to abstract away unnecessary details in the construction. The lattice stabilizer checks that implement the defects we introduce can be found in Section VI.

The abstract picture for the surface code is a patch of $\mathcal{Z}(\text{Vec}_{\mathbb{Z}_2})$ topological order which supports anyon types $\{1, e, m, \psi\}$ together with a pair of e -condensing horizontal, and m -condensing vertical, gapped boundaries arranged as shown in Figure 5. See Section II for basic background information on surface code and its TQFT features including anyons, defects and boundaries.

A logical $\overline{Z}\overline{Z}$ stabilizer can be enforced on a pair of surface codes by introducing a topological defect line that allows the pair of \overline{Z} string operators to condense². This is satisfied by a defect along the \hat{z} direction that condenses the Lagrangian subgroup of anyons generated by $\langle e_1^\ell e_2^\ell, e_1^r e_2^r, e_1^\ell e_1^r, m_1^\ell m_1^r m_2^\ell m_2^r \rangle$ where 1, 2 labels the layer and ℓ, r labels the region to the left, right of the defect.

We remark that this is not an invertible defect, and also does not factor into a pair of gapped boundaries. Above we have used the folding trick to view the line defect as a gapped boundary of four half planes of $\mathcal{Z}(\text{Vec}_{\mathbb{Z}_2})$ topological order. For stacks of $\mathcal{Z}(\text{Vec}_{\mathbb{Z}_2})$ topological order, a Lagrangian subgroup of condensing anyons can be described compactly by a set of independent generators, which have trivial self and mutual braiding statistics, with size equal to the number of toric codes that terminate at the gapped boundary.

² The connection between anyon condensation and measurement has been explored recently in Refs. [97, 110, 111].

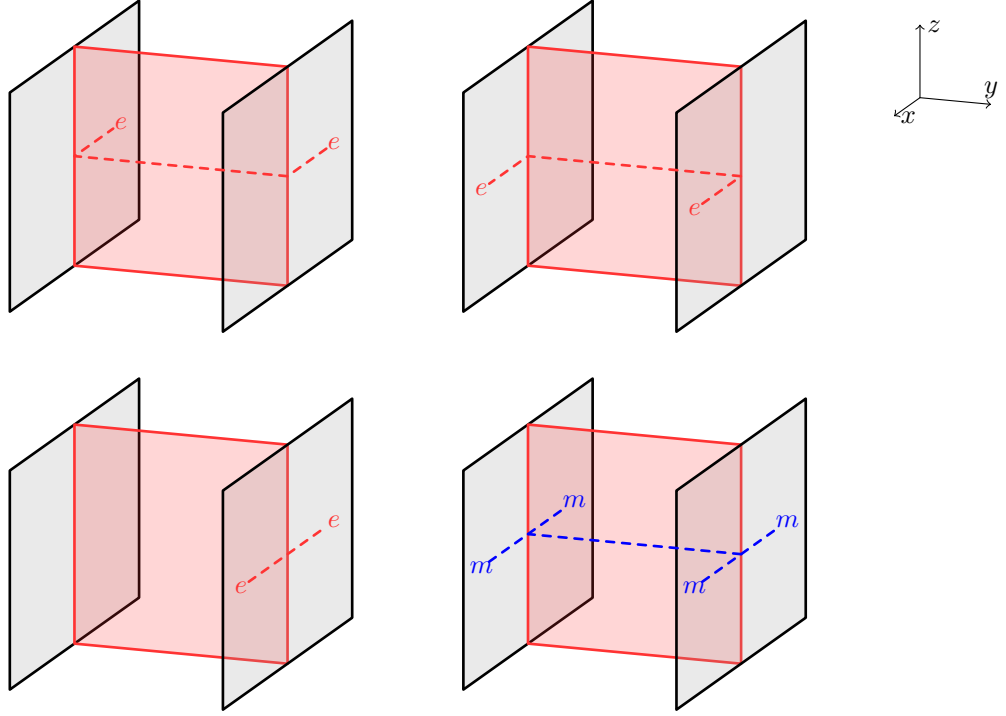


FIG. 9. Each grey layer is a surface code patch with the boundary conditions specified in Figure 5. We refer to the grey layers as xz layers. The red layer corresponds to a topological defect emulating a $\bar{Z}\bar{Z}$ stabilizer between the two xz layers. We refer to the red layers as yz layers. The red layer condenses $\langle e_1^\ell e_2^\ell, e_1^r e_2^r, e_1^\ell e_1^r, m_1^\ell m_1^r m_2^\ell m_2^r \rangle$.

The above topological defect is only local if the pair of surface code layers involved are within a constant distance of each other. Generalizing this construction to allow concatenation with codes that are not spatially local requires an extra trick. This is provided by decomposing the above topological defect into a pair of topological defects joined by an additional layer of surface code that runs between the original surface code layers, see Figure 9. This results in a pair of topological defects where a triple of $\mathcal{Z}(\text{Vec}_{\mathbb{Z}_2})$ topological orders meet, see Figure 10. The new pair of line defects are specified by the condensed anyons $\langle e_1^\ell e_1^r, e_1^\ell e_{\bar{z}}, m_1^\ell m_1^r m_{\bar{z}} \rangle$ and $\langle e_2^\ell e_2^r, e_2^\ell e_{\bar{z}}, m_2^\ell m_2^r m_{\bar{z}} \rangle$ respectively, which are equivalent up to a relabelling of the anyons.

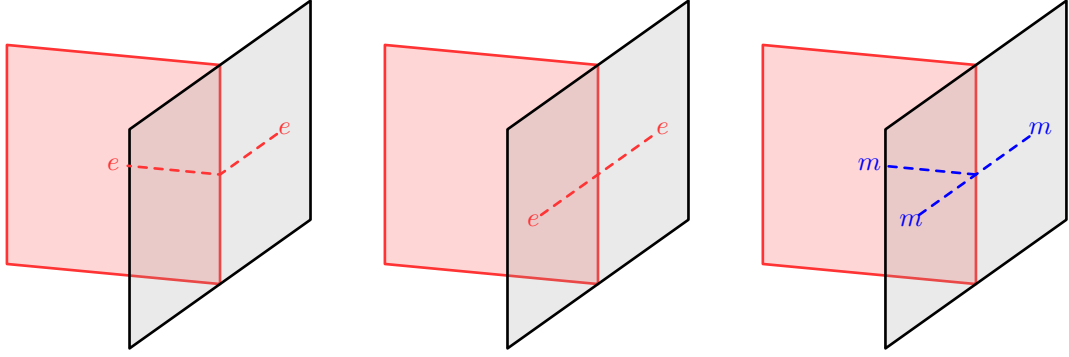


FIG. 10. Topological defect trijunction between a zy layer and an xz layer that condenses $\langle e_1^l e_1^r, e_1^l e_z, m_1^l m_1^r m_z \rangle$.

C. Repetition code example.

It is convenient at this point to illustrate our discussion with a specific example. Here we describe the layer code that corresponds to taking the 3-qubit repetition code $\mathcal{S} = \langle Z_1 Z_2, Z_2 Z_3 \rangle$ as input. This layer code is given by two pairs of the defects in Figure 10 connecting together a triple of surface code layers as shown in Figure 11. This layer code displays an example of the topological defect network structure inherent to all layer codes. That is, it is formed by layers of surface code, joined together by topological defect line junctions according to the Tanner graph of the input repetition code.

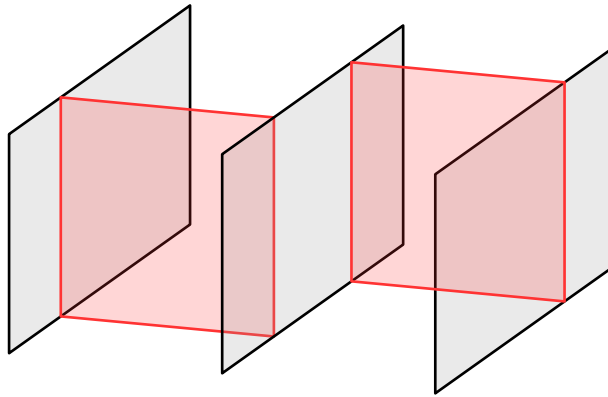


FIG. 11. Topological defect network emulating the concatenation of a surface code and a repetition code. It is composed of three xz layers, each representing a qubit of the repetition code, and two yz layers, each representing a check of the repetition code.

In this layer code, the \hat{y} boundaries of the yz -oriented surface codes are taken to be e -condensing.

With this choice, all boundaries ending on a yz -plane match and are e -condensing. Due to the defects, the Z string operator in each layer provides an equivalent logical \bar{Z} representative. On the other hand, the X string operator in an individual layer no longer preserves the code space as it creates an additional excitation when it pierces the newly introduced line defects. A logical \bar{X} representative of the concatenated code is found by connecting together the product of the X string operators in the original three surface code layers with additional string operators that remove the excitations that appear at the junctions, see Figure 12.

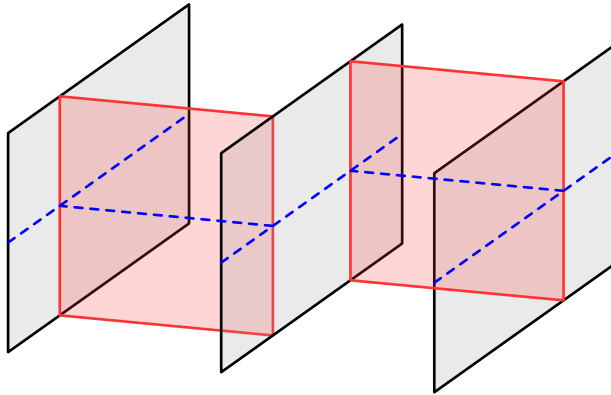


FIG. 12. Topological defect network emulating the concatenation of a surface code and a repetition code. The network enforces that the logical \bar{X} operator has the same structure as that of the concatenated code, without the need for high weight long range interactions.

D. Generalizing the construction.

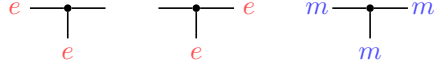
To generalize the above construction to Shor's code, and beyond to general CSS codes, we need to introduce several further features:

1. Defects that implement k -body X , or Z , stabilizer checks.
2. Line defects that resolve the crossing of xy and yz oriented surface code layers.
3. Point defects where multiple line defects meet.

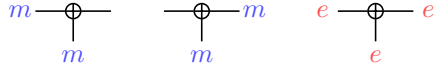
Item 3. above captures point defects where a line defect meets a boundary. This is because gapped boundaries of copies of the surface code can be viewed as line defects.

E. k -body terms.

To address the first two items above it is convenient to introduce an abstract picture for a line defect that captures the anyons it condenses while ignoring the homogeneous structure along the defect. For the $\langle e_1^\ell e_1^r, e_1^\ell e_z, m_1^\ell m_1^r m_z \rangle$ defect this picture is



we henceforth refer to this defect as the \bullet -defect. This defect can be generalized to an arbitrary number k of incoming layers by joining together $(k-2)$ \bullet -defects with three incoming layers each. It is easy to verify that the order does not matter. Due to the symmetry of $\mathcal{Z}(\text{Vec}_{\mathbb{Z}_2})$ under exchanging e and m , there is a related defect with the condensation rules



we refer to this as the \oplus -defect. Following the discussion for the \bullet -defect above, the \oplus -defect generalizes straightforwardly to any number of incoming layers.

By combining the above defects we can implement the k -body generalization of the concatenated Z stabilizer check. This is depicted in Figure 13, where we make use of the decomposition of a k -layer \oplus -defect into trivalent \oplus -defects to rearrange the network into one defect per xy -surface code layer, connected by an auxiliary layer of yz -surface code³. An analogous construction for concatenated X stabilizer checks is achieved by exchanging the roles of the \bullet - and \oplus - defects in Figure 13.

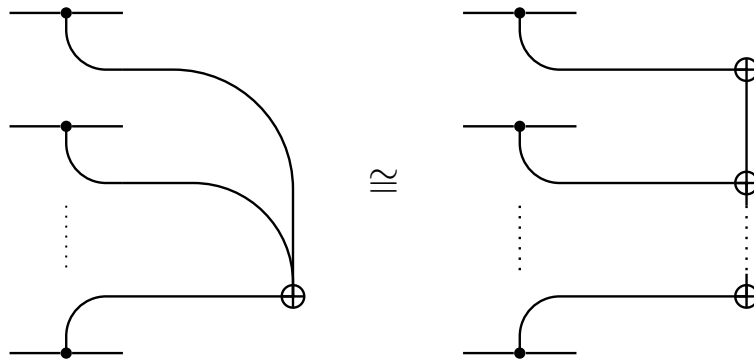


FIG. 13. Decomposition of a defect corresponding to a single k -body check into to a string of defects corresponding to at most 3-body checks.

³ This decomposition is closely related to Shor's scheme for syndrome extraction [8].

We have now answered item 1. from the list in Section III D as we have a recipe to implement k -body X , or Z , stabilizer checks on layers of surface code using defects that are local in 3D. The defects involved in a Z stabilizer check are shown in Figure 14, and those involved in an X stabilizer check are shown in Figure 15.

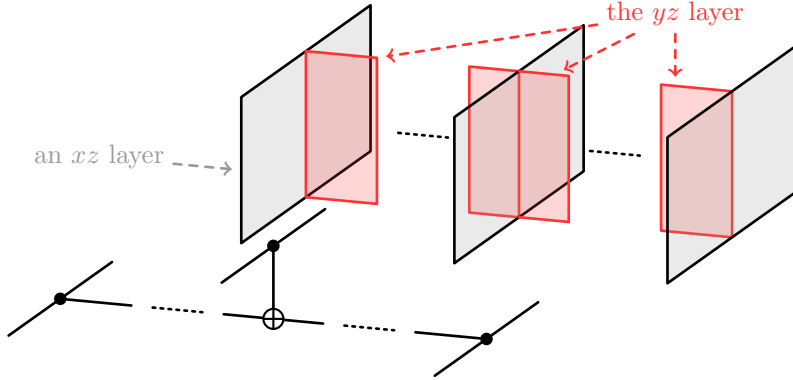


FIG. 14. Defects associated with an arbitrary k -body Z -check. The network of surface code and defects corresponding to this check is referred to as a yz layer. Such defects are illustrated as red layers in yz planes below.

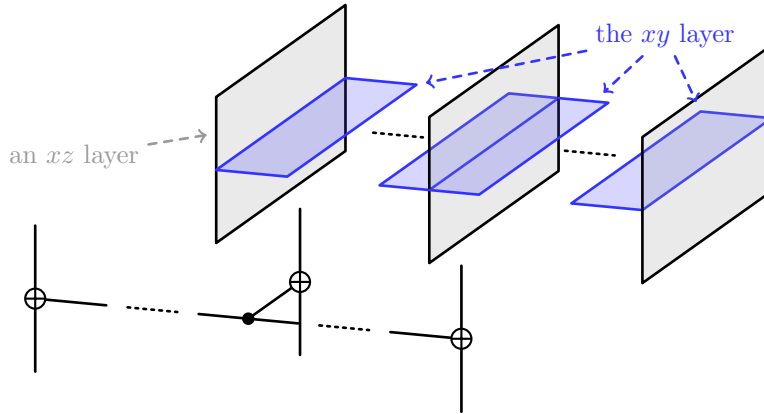


FIG. 15. Defects associated with an arbitrary k -body X -check. The network of surface code and defects corresponding to this check is referred to as an xy layer. Such defects are illustrated as blue layers in xy planes below.

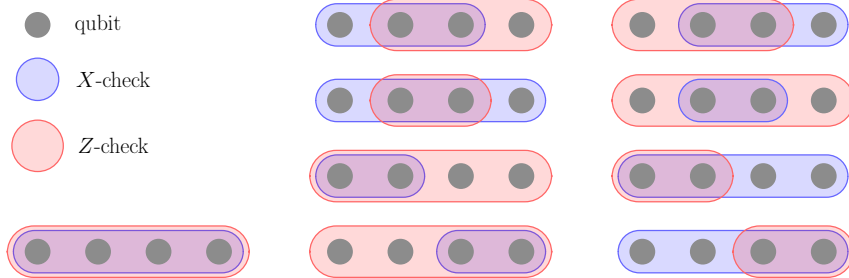
These defects serve to introduce equivalences on Z , respectively X , string operators that correspond to multiplication by the associated stabilizer check operator. Additionally, they introduce an energy penalty for any X , respectively Z , string operator that passes through the defect. Only an even number of X , respectively Z , string operators can pass through a defect on surface code

layers that it interacts with without leaving the codespace. This is because each such string operator deposits an excitation on the defect, which can be paired up and annihilated if their number is even, see Figure 12.

F. Line defects at the intersection of xy and yz layers

Our construction for a general CSS code involves defects coupled to xy planes that implement concatenated X checks, as well as defects coupled to yz planes that implement concatenated Z checks. For xy and yz planes that do not interact with any common xz layers, corresponding to X and Z checks that have nonoverlapping support, any lines of intersection along \hat{y} are taken to be trivial crossings. On the other hand, for an xy and yz layer that intersect nontrivially on, necessarily an even number of, common xz layers the above trivial crossing along \hat{y} does not suffice. To see why this is the case, we note that a Z string operator in an xz surface code layer is equivalent to one, or two, Z string operators in any yz layer that meets the xz layer at a nontrivial defect. If the yz layer were to intersect trivially with all xy layers, the Z string operators therein are free to pass across the full system while preserving the codespace, thereby implementing undesired logical string operators.

To find appropriate \hat{y} defect lines we introduce additional structure to the checks of the input CSS code. We consider qubits laid out along a line, and note there are 9 inequivalent configurations for an overlapping X and Z check in total.



We remark that the following pair of single qubit overlaps are not possible as the X and Z checks commute and hence must share an even number of qubits.

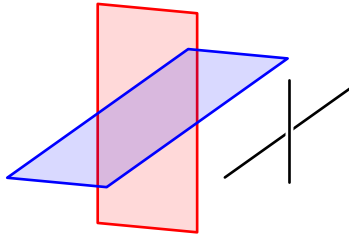
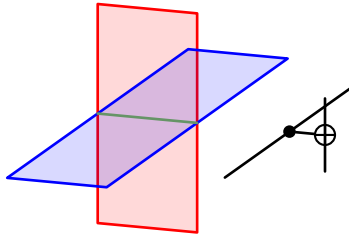


The extra structure we make use of in our defect network construction is a pair matching on the qubits that are contained within the support of each overlapping pair of X and Z checks. This pair matching is depicted by green lines in the example below.



This pairing is defined by the linear ordering of the qubits in the general input CSS code that have been arranged along a line. The qubits in the intersection of the supports of an X and Z check are then grouped into pairs following this ordering, depicted by green lines above.

The choice of \hat{y} defect lines in the layer code relies on the additional pairing data. Along the \hat{y} intersection line of an xy and yz layer we introduce nontrivial line defects that run between xz layers corresponding to input qubits that have been paired. The remaining unpaired \hat{y} line segments are left as trivial crossing defects.



It is now easily verified that a Z string operator within an xz plane and its equivalent Z string operators within yz planes create equivalent excitations, up to local string operators. An analogous property holds for X string operators. This resolves item 2. from the list in Section III D.

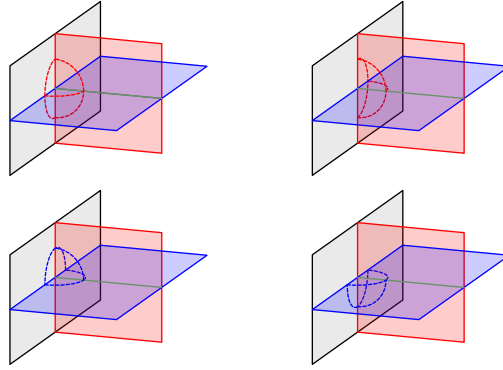
G. Point defects

We now address point 3. from the list in Section III D. Recall that point defects in copies of the surface code are fixed by their eigenvalues under the codespace preserving topologically nontrivial operators supported on an annulus surrounding the point, see Section II. Below, we demonstrate a complete set of local topological operators whose eigenvalues fully specify the point defects that appear in the layer code construction.

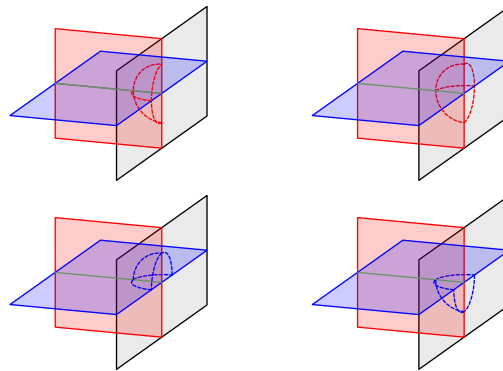
Bulk

We first consider point defects within the bulk of the layer code. We remark that the list below does not contain trivial intersections, where layers simply pass through one another, as those decompose into standard annulus algebras of the individual $\mathcal{Z}(\text{Vec}_{\mathbb{Z}_2})$ layers.

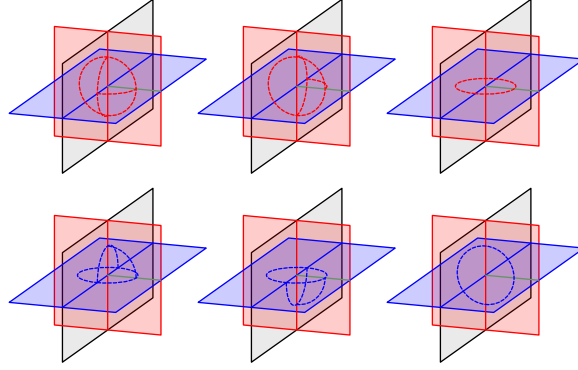
1. The first point defect configuration corresponds to an xy and yz layer ending on the same xz layer. There are four incoming half planes of $\mathcal{Z}(\text{Vec}_{\mathbb{Z}_2})$ topological order and hence four independent topological operators in the shell around the point suffice to lift all degeneracy:



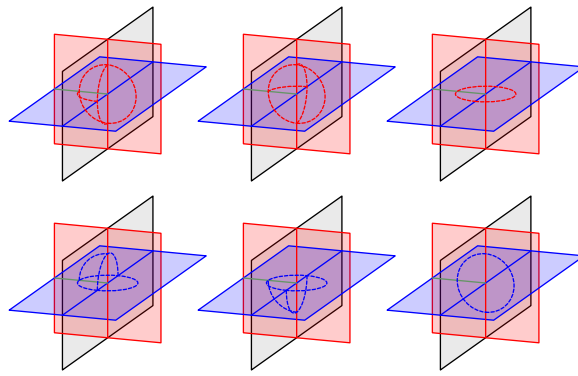
2. The second point defect is simply the reflection of the 1st through an xz plane:



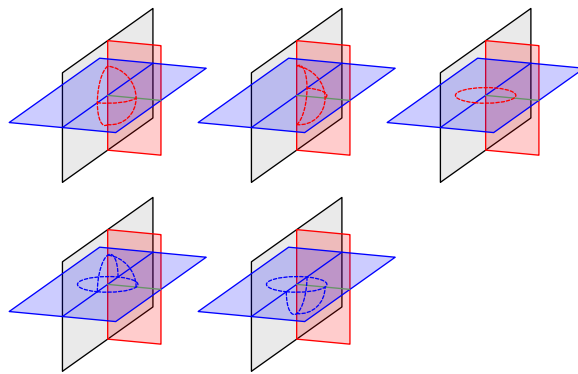
3. The third point defect configuration corresponds to an xy and yz plane interacting with a common xz layer, but not ending there. A nontrivial \hat{y} defect ends on the point from above. Here there are 6 incoming planes of $\mathcal{Z}(\text{Vec}_{\mathbb{Z}_2})$ and hence we find 6 independent topological operators in the shell around the point:



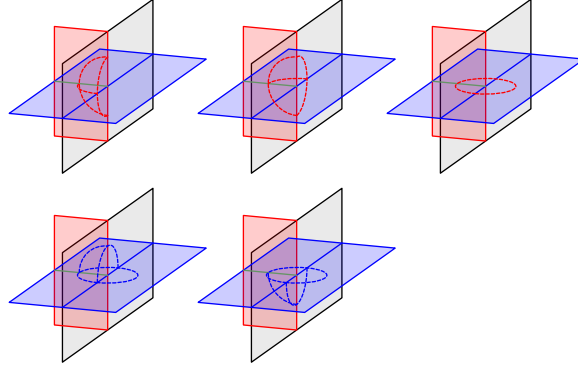
4. The fourth point defect configuration is a reflection of the 3rd through an xz plane:



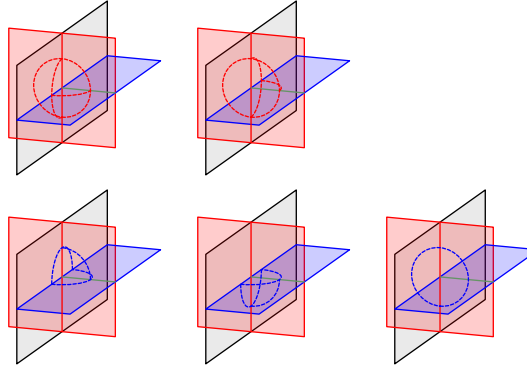
5. The fifth point defect configuration corresponds to an xy plane interacting with an xz plane that a yz plane ends on from above. This necessitates a nontrivial \hat{y} defect also ending on the point from above. There are 5 half planes of $\mathcal{Z}(\text{Vec}_{\mathbb{Z}_2})$ meeting at the point defect, and hence we find 5 independent topological operators in the shell:



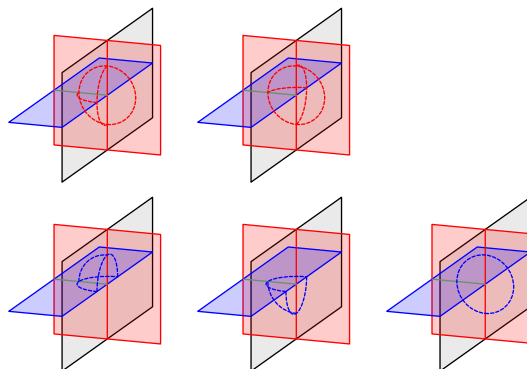
6. The sixth point defect configuration is a reflection of the fifth through and xz plane:



7. The seventh point defect configuration is similar to the fifth. Here a yz plane interacts with an xz plane that an xy plane ends on from above. Again this requires a nontrivial \hat{y} line defect to end on the point from above. There are 5 half planes of $\mathcal{Z}(\text{Vec}_{\mathbb{Z}_2})$ meeting in this configuration, hence we find 4 independent topological operators:



8. The eighth and final bulk configuration is simply the reflection of the seventh through an xz plane:

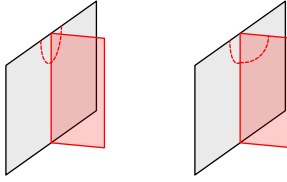


This concludes the enumeration of bulk point defects.

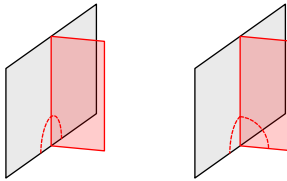
Boundary

We now consider point defects that sit on the boundary of the layer code. We remark that the list below does not contain the boundary point defect where two layers cross trivially, as that decomposes into a pair of standard surface code boundaries.

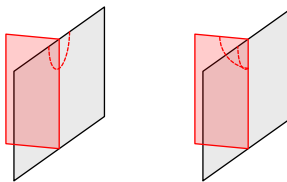
1. The first boundary point defect configuration corresponds to the front xy boundary of a yz layer ending on an xz plane. There are two half planes of $\mathcal{Z}(\text{Vec}_{\mathbb{Z}_2})$ meeting the boundary at this point defect and hence we find a pair of independent topological operators:



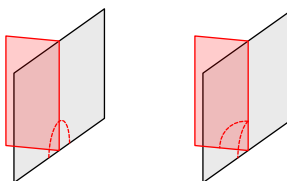
2. The second boundary point defect configuration is a reflection of the first through an xy plane:



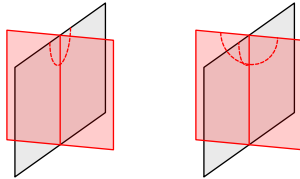
3. The third boundary point defect is the reflection of the first through an xz plane:



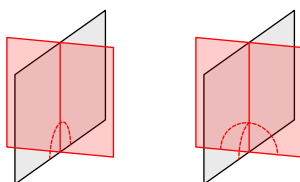
4. The fourth boundary point defect is the reflection of the second through an xz plane:



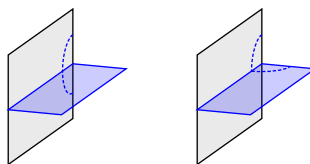
5. The fifth boundary point defect configuration corresponds to the front xy boundary of a yz layer interacting with an xz plane nontrivially. There are two half planes of $\mathcal{Z}(\text{Vec}_{\mathbb{Z}_2})$ ending at this point and hence we find a pair of independent topological operators:



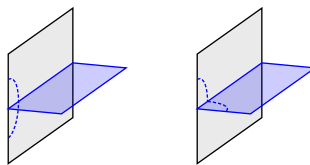
6. The sixth boundary point defect is the reflection of the fifth through an xy plane:



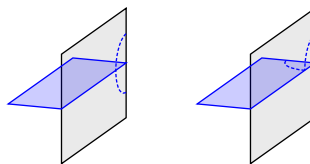
7. The seventh boundary point defect configuration corresponds to the left yz boundary of an xy layer ending on an xz layer. There are two planes of $\mathcal{Z}(\text{Vec}_{\mathbb{Z}_2})$ meeting at this point and hence we find a pair of independent topological operators:



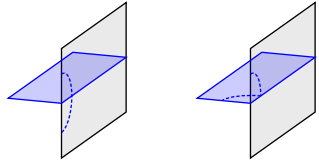
8. The eight boundary point defect configuration is the reflection of the seventh through an yz plane:



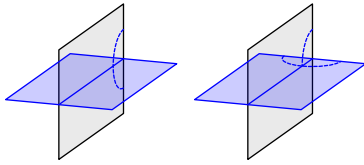
9. The ninth boundary point defect configuration is the reflection of the seventh through an xz plane:



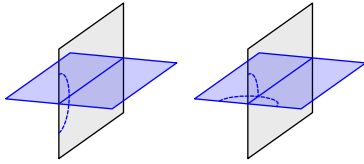
10. The tenth boundary point defect configuration is the reflection of the 8th through an xz plane:



11. The eleventh boundary point defect configuration corresponds to the left yz boundary of an xy layer interacting nontrivially with an xz layer. There are two half planes of $\mathcal{Z}(\text{Vec}_{\mathbb{Z}_2})$ meeting the defect and accordingly we find a pair of independent topological operators:



12. The twelfth, and final, boundary point defect configuration is the reflection of the eleventh through a yz plane:



This concludes the enumeration of boundary point defects in the layer code construction.

IV. CODE PROPERTIES

In this section we explain some of the essential features of the layer codes that are output by the construction above.

A. Code Parameters

First, we explain the code parameters that are achieved by the layer code construction. The construction maps the code parameters of an arbitrary input CSS code to an output layer code as follows

$$[[n, k, d]] \mapsto [[\Theta(nn_Xn_Z), k, \Omega(\frac{1}{w}d \min(n_X, n_Z))]]. \quad (11)$$

Here n_X is the number of X checks, n_Z the number of Z checks, and w the maximum weight of the checks in the input code. The output code is local in three dimensional space and has checks of weight 6 or less. When a good CSS LDPC code is taken as input, the output code achieves parameters $[[N, \Theta(N^{\frac{1}{3}}), \Theta(N^{\frac{2}{3}})]] = [[\Theta(L^3), \Theta(L), \Theta(L^2)]]$, where L is the linear extent of the system. These code parameters are optimal in the sense that their scaling saturates the BPT bound for three spatial dimensions.

Below we discuss the scaling of the code parameters $[[N, K, D]]$ of the layer code that is produced when our construction is applied to an input code with parameters $[[n, k, d]]$.

1. Number of Physical Qubits: $N = \Theta(nn_Xn_Z)$

The scaling of the number of physical qubits in the output code is lower bounded by the number of physical qubits in n layers of surface code with linear dimensions $cn_X \times cn_Z$. Here c is a constant that sets the superlattice spacing between the surface code layers involved in the construction. On the other hand, N is upper bounded by the number of physical qubits in a stack of surface codes along the three lattice directions of a $cn \times cn_X \times cn_Z$ cuboid.

This gives

$$2c^2nn_Xn_Z \leq N \leq 6c^3nn_Xn_Z \quad (12)$$

and hence $N = \Theta(nn_Xn_Z)$.

2. Number of Logical Qubits: $K = k$

The number of logical qubits in the output code is equal to the number of logical qubits in the input code. To demonstrate this we consider a basis of representatives for the logical operator pairs in the input code

$$\left\{ \overline{X}_i, \overline{Z}_i \mid \{\overline{X}_i, \overline{Z}_i\} = 0, [\overline{X}_i, \overline{Z}_j] = 0, \text{ for } i \neq j, i, j = 1, \dots, k \right\}, \quad (13)$$

where the \overline{X}_i operators are products of physical X operators, and \overline{Z}_i operators are products of physical Z operators. Here $\{A, B\} = AB + BA$ denotes the anticommutator and $[A, B] = AB - BA$ denotes the commutator. For each $\overline{X}_i, \overline{Z}_i$, logical operator pair in the input code there is a corresponding logical operator pair \tilde{X}_i, \tilde{Z}_i , in the output layer code.

We define a *concatenated representative* for the \overline{X}_i logical in the layer code by replacing each physical X in the input code with an X string operator across the corresponding xz surface code

layer. We remark that this concatenated representative operator would be a logical operator in a straightforward concatenation of surface code with the input code. However this concatenated representative is *not* a logical operator in the layer code, as the string operators violate stabilizers on the yz Z -check layers that meet the relevant xz qubit surface code layers at nontrivial junctions. The number of such excitations created in each yz layer must be even. This is because the incidence relation of the string operator in each xz surface code layer with the yz layers via nontrivial junctions matches the incidence relation of the corresponding input physical qubit with the input Z checks. Hence the incidence of a concatenated representative operator on a yz layer at nontrivial junctions matches the incidence of the relevant input logical on the associated input Z check, which must be even as they commute. We can then pair up the excitations within each yz plane and remove all nontrivial syndromes via X string operators within yz planes to form a logical operator \tilde{X}_i that we call a *quasiconcatenated representative*. See Figure 12 for a depiction of a quasiconcatenated logical operator in a repetition code example.

A quasiconcatenated representative for each \tilde{Z}_i logical is obtained similarly with yz planes replaced by xy planes, and X string operators replaced by Z string operators. This construction preserves the commutation relations of the logical operators. To see this we note that the first step of the process, mapping single qubit Pauli operators to string operators in layers of surface code, preserves commutation relations. The second step of the process, in which excitations are paired up in yz and xy layers, does not affect the commutation relations. This follows from the fact that the X operators within the yz and the Z operators within the xy planes can be taken to have disjoint support, respectively.

To complete the proof that $K = k$ we must demonstrate both that there are no additional logical operators that have not been accounted for, and that none of the logical pairs in the output code we have counted are equivalent, up to multiplication with stabilizers. These statements follow from the characterization of the logical operators in Section V, summarized in Remark 4.

$$3. \quad \text{Distance: } D = \Omega\left(\frac{1}{w}d \min(n_X, n_Z)\right)$$

We now discuss a lower bound on the weight of the quasiconcatenated representative logical operators. The results in Section V establish that this lower bound holds for the scaling of the code distance, see Corollary 2.

We start by considering the quasiconcatenated representative logical operators \tilde{X}_i in the output layer code. These operators are obtained from logical operators \overline{X}_i in the input code by replacing

each of their physical X operators by X string operators on the corresponding xz surface code layer and applying additional string operators in the yz layers to pair up the excitations that the string operators in the xz layers create. The weight of the quasiconcatenated representative is bounded from below by dcn_Z . However, the addition of the xy layers introduce new equivalence relations for these logical operators that allow string operators on xz layers that meet an xy layer at nontrivial junctions to be moved onto the xy layer. In the input code this corresponds to the associated logical operator \overline{X}_i sharing support with part of an X stabilizer check. Assume we have a minimum weight logical operator representative \overline{X}_i . The common support of this logical operator representative with any X stabilizer must be $\leq \frac{w}{2}$, otherwise there would be an equivalent representative logical operator with lower weight thus contradicting the minimum weight assumption. The worst-case weight reduction via the new equivalence relations due to xy layer mentioned above can only result in the weight being multiplied by $\frac{2}{w}$. This corresponds to all of the quasiconcatenated representative's string operators in xz layers being cleaned into xy layers. Hence the weight lower bound retains the same scaling with n , given by $\Omega(\frac{2}{w}dcn_Z)$, provided that the input code is LDPC.

In the case that the input code is not LDPC, we remark that the X distance of the output code still satisfies $\Omega(cn_Z)$. This is simply because the logical operators remain string-like in the output layer code.

Analogous statements hold for the Z logical operators of the output code.

The characterization of logical operators in Section V implies that the lower bound on the logical weight introduced above holds for any equivalent logical operators in the output layer code, see Corollary 2. This accounts for equivalence under all stabilizers, going beyond the simple cleaning process outlined above.

B. Energy barrier

In this subsection we demonstrate that the logical energy barrier of the output layer code Δ_{out} is lower bounded by a ratio of the logical energy barrier of the input code Δ_{in} to the product of maximum stabilizer weight w with the maximum number of checks that act on a common qubit \hat{w} in the input code

$$\frac{4\Delta_{\text{in}}}{w\hat{w}} \leq \Delta_{\text{out}}. \quad (14)$$

We first remark that the energy barrier of the output code is upper bounded by the energy

barrier of the input code plus 1. This follows by considering, without loss of generality, a sequence of Pauli X operators in the input code that attain its energy barrier and implement a nontrivial logical operator. Each individual Pauli X operator in this sequence can be mapped to a Pauli X string operator in the output code that can be sequentially implemented at the cost of at most one additional unit of energy on top of the energy penalty of the input X operator. As Pauli X string operators are sequentially implemented on the layer code, we can maintain a maximum of a single excitation within each yz layer. This can be achieved by using string operators to move any excitation within a yz layer to the appropriate location that will immediately annihilate any additional excitation that would be created in that layer via sequential application of an X string in some xz layer. This process results in the implementation of a quasiconcatenated logical operator in the layer code with the claimed energy penalty, which is hence an upper bound on the energy barrier Δ_{out} . A similar argument applies for Pauli Z logical operators.

To derive a lower bound on the energy barrier we devise a method to convert any sequence of Pauli Z operators in the layer code into a different sequence that can be used to define a sequence of Pauli Z operators on the input code. This conversion increases the energy penalty multiplicatively by at most a factor $w\hat{w}$, where w is the max weight of a stabilizer check and \hat{w} is the maximum number of checks that act on a common qubit in the input code. Hence for input codes that are LDPC, the energy barrier of the output layer code retains the same scaling with n as the energy barrier of the input code.

We now describe the conversion process for a multi-qubit Pauli Z operator in a layer code. First, all e excitations within yz layers are transformed into e excitations on xz layers via string operators along the \hat{y} direction. There are two choices per yz layer at this step, we take the one that produces the minimum number of excitations. This step increases the energy penalty multiplicatively by at most $\frac{w}{2}$. Next, we apply string operators to move all e excitations within xz layers to condense at a rough boundary on an external xy face of the cuboid containing the layer code. Again there are two choices at this step for each e excitation, we take the choice that produces the minimum number of excitations. This step increases the energy penalty multiplicatively by at most $\frac{\hat{w}}{2}$. At this point, all remaining e excitations are on xy layers. We then apply string operators to bring all e excitations on each xy layer to a common point. This step does not increase the energy penalty. The results in Section V establish that the Pauli operator produced by this procedure is equivalent to a quasiconcatenated operator that consists of up to one Z string operator per xz layer, connected by strings in xy layers. Each such quasiconcatenated string operator defines a multi-qubit Pauli Z operator on the input code by mapping each Z string operator in an xz layer

to the Z operator on the associated input physical qubit.

Via the above mapping, any sequence of Pauli Z operators on the output code maps to a sequence of Pauli Z operators on the input code. For an LDPC code, a local change to the operator on the output code maps to a local change to the operator on the input code⁴. This is because the operator conversion process for a syndrome on any layer only involves other layers that meet the original layer at a nontrivial junction. Hence, a local sequence which implements a logical operator on the output code produces a local sequence which implements a logical operator on the input code. In doing so the energy penalty on the output code is increased multiplicatively by at most a factor $\frac{1}{4}w\hat{w}$, and hence the energy barrier of the output code must satisfy the lower bound

$$\frac{4\Delta_{\text{in}}(n)}{w\hat{w}} \leq \Delta_{\text{out}}(n). \quad (15)$$

Here we are considering the less restrictive definition of the energy barrier that allows a sequence of local Pauli operators to be applied, see Section II. This result implies that the layer code construction preserves the scaling of the energy barrier with n for LDPC codes. We remark, however, that since our construction increases the number of physical qubits from n to $\Theta(n_{X}n_{Z})$ the ratio of the energy barrier divided by the number of physical qubits is generically decreased by the layer construction.

C. Stabilizer check relations

In this subsection we demonstrate that relations between the stabilizer checks of the input code imply similar relations for the output code. This implies that the excitations in the output code inherit conservation laws from the excitations in the input code [15, 65, 112].

A relation \mathcal{R} amongst X checks on the input code

$$\prod_{i \in \mathcal{R}} S_i^X = \mathbb{1}, \quad (16)$$

implies a similar relation on the output code. This follows by considering the product of the X checks on xy layers that correspond to the input checks appearing in the relation \mathcal{R} . The product of all X checks on an xy layer results in a quasiconcatenated representative of the associated X check in the input code. This operator involves a product of X string operators on each xz layer that corresponds to a qubit in the support of the associated input X check. These string operators are

⁴ Here local refers to combinatorial k -locality for a constant k .

connected by string operators where the xy layer intersects yz layers at nontrivial junctions. Hence the product of all X checks on all xy layers involved in an input relation yields an even number of X string operators on each xz layer, together with additional connecting string operators on the yz layers that are intersected nontrivially. We then pair up the X string operators in each xz layer, following the ordering of the xy layers they originate from, and multiply by the X checks in the xz layer on the regions enclosed by the paired up strings. This leaves no nontrivial operators on the xz layers, due to the smooth boundary conditions on the yz boundaries of the cuboid. This step does create additional X string operators on the yz layers that intersect the regions between the paired up strings. These string operators, together with the other string operators in the yz layers from the initial step, form \mathbb{Z}_2 boundaries of regions within the yz planes. We then multiply by X checks within these regions of the yz planes to cancel out the string operator along their boundaries. This completes the trivialization of the operator, and hence we have constructed a relation inherited from any relation of the input code.

A relation in the input code also implies the presence of certain string-like stabilizers in the output code. Consider a relation \mathcal{R} satisfied by X checks

$$\prod_{i \in \mathcal{R}} S_i^X = \mathbb{1}. \quad (17)$$

An X string operator spanning an xy layer in the \hat{y} direction creates an m excitation on each xz layer that meets it at a nontrivial junction. The product of these string operators for all xy layers corresponding to X checks in a relation hence produces an even number of m excitations on each xz layer which can then be paired up via additional string operators in the xz layers. To demonstrate that this is a stabilizer, we notice that this string-like operator can be deformed through any yz layer. The string-like operator can hence be moved to a yz boundary of the cuboid and condensed, i.e. trivialized via multiplication with smooth boundary stabilizers.

V. PROOF OF MAIN RESULTS

In this section we present a number of lemmas that characterize the structure of logical operators appearing in the output layer codes. These results are relied upon when establishing the code properties in the previous section.

A. Characetrization of logical operators

We focus our discussion on X logical operators, analogous results hold for Z logical operators. Our strategy is to consider dividing up \overline{X}_i logicals into segments that are each supported within a thin slab that contains a single yz layer. The product of all slabs, along with a pair of boundary slabs, then reproduces the complete logical. A similar approach applies to dividing \overline{Z}_i logicals into thin slabs that each contain a single xy layer.

We first consider collections of m excitations that can be supported on the boundary between a pair of slabs. We remark that such a boundary must fall between a pair of yz layers. Such collections of m excitations have natural equivalence relations under stringlike X operators supported on the same boundary. String operators confined to the intersection of an xz plane with the boundary, or the intersection of the boundary with an xy plane away from a nontrivial junction, can be used to reduce a collection of m excitations to a *configuration* that consists of at most one m excitation on each such intersection line.

Definition 1. *A configuration of m excitations on one boundary of a yz slab is defined by a binary variable for each xz layer, and each segment of xy layer between a pair of nontrivial junctions.*

Next we consider the equivalence of m configurations on a single boundary induced by the condensation or creation of m excitations at nontrivial junctions that intersect that boundary. These equivalences can be implemented by products of string operators on the intersection of the boundary with xz and xy layers that create no excitations at the nontrivial junctions.

Definition 2. *A pair of m configurations on the boundary of a yz slab is equivalent if they can be related by a sequence of m condensations or creations at nontrivial junctions.*

Remark 1. There is at least one representative for every equivalence class of m configurations that has no m excitations on any xy layers. Next we remark that configurations of m excitations that are supported exclusively on xz planes meeting the boundary can be formally mapped to X operators on the qubits of the input code. This mapping simply sends such a configuration of m excitations to a multi-qubit Pauli X operator that is given by a product of single-qubit Pauli X operators on each qubit of the input code that corresponds to an xy layer with an m excitation on it. An equivalence between a pair of excitation-free xy layer representatives maps to an equivalence between their associated multi-qubit Pauli operators under multiplication with an X stabilizer of the input code.

We now consider how much the weight of an excitation-free xy layer m configuration can be reduced by moving their m excitations into xy layers.

Remark 2. The equivalence relations on m configurations allow m excitations on xz layers to be moved into xy layers. Each m excitation in an xy layer is equivalent to m excitations on xz layers that correspond to qubits in the support of a partial X stabilizer of the input code. Consider an excitation-free xy layer m configuration corresponding to an X operator in the input code with minimal weight d amongst its equivalence class up to multiplication with X stabilizers of the input code. The weight of such an m configuration is lower bounded by $\geq \frac{2}{w}d$ under the equivalence relation in Definition 2. This is because each X check in the input code has maximum overlap $\leq \frac{w}{2}$ with the minimal weight X operator, otherwise multiplication with that X check would reduce the weight further.

Next, we turn our attention to the relationship between the configuration of m excitations supported on one boundary of a slab to the other.

Lemma 2. *Consider an X operator in a yz slab that creates no excitations on the xy and xz layers in the bulk of that slab. The configuration of m excitations created by this operator on one boundary of the slab is equivalent to the configuration created on the other boundary.*

Proof. First, any excitations within the yz layer contained in the slab can be moved onto the intersection of the yz layer with an xy plane via X string operators supported on the yz layer. This process creates no further excitations. Without loss of generality, we consider an X operator that creates no excitations in the bulk of the slab except in the yz layer where it intersects a chosen xy plane. Such an X operator can be cleaned onto the single chosen xy plane by multiplication with stabilizers in the layer code. In particular, we can pick this xy plane to sit between xy layers of the code. The resulting cleaned operator is a product of string operators whose support is contained within the intersection of the chosen xy plane with the xz layers and the yz layer in the slab, see Figure 12 for an example. Since the cleaned operator creates no excitations on the xz layers within the slab, it must either have no support on a given xz layer or have support on the whole intersection of that xz layer with the chosen xy plane. This results in all m excitations on one of the slab boundaries having a partner with the same yz coordinates on the other boundary. \square

Remark 3. We remark that the parity of the m excitations left on the yz layer in the slab matches the anticommutation relation of the associated many-qubit Pauli X operator with the relevant Z check in the input code. We also remark that the configuration of m excitations on a boundary of

a yz slab is only defined up to the equivalence relation in Definition 2 if we allow the application of X operators at that boundary.

Lemma 3. *The configuration of m excitations created on either boundary of a yz slab by the restriction of a logical X operator to that slab must be in an equivalence class that corresponds to a logical X operator of the input code under the mapping in Remark 1.*

Proof. We begin by remarking that a straightforward mapping of X operators on the input code to string operators on xy planes that run across a yz slab results in an operator that creates a number of m excitations on the yz layer whose parity matches the stabilizer syndrome of the corresponding input Z check. These m excitations can all be fused at a common location in the yz layer via string operators, producing at most a single m excitation. For there to be no m excitation, the configuration of m excitations on the boundary of that slab must be in an equivalence class that corresponds to an X operator on the input code that commutes with the relevant Z check. Hence the restriction of a layer code logical X operator to any slab must create a configuration of excitations at the boundary that corresponds to a logical X operator on the input code. This is because the layer code logical X operator must create no excitation on any yz slab. To complete the proof, we demonstrate below that a nontrivial logical X operator in a layer code must have support on all slabs. \square

Lemma 4. *An X logical operator on a layer code that is supported wholly within a yz slab must be a stabilizer.*

Proof. An X logical supported on a single yz slab is a product of string operators on the layers within the slab, joined at the nontrivial junctions. The string operators can be cleaned off the xy layers by multiplication with stabilizers. Within xz layers and the yz layer, m string operators can be deformed along the z direction via multiplication with stabilizers. Hence the X logical can be cleaned onto a single xy plane via stabilizer multiplication. This must result in a trivial operator given the support and the fact that no excitations are created. \square

Corollary 1. *A nontrivial X logical operator must have nontrivial support on all yz slabs.*

Proof. Consider an X logical operator that acts trivially on some yz slab. It can be written as a product of disjoint X logical operators on either side of that yz slab. The excitations created by cutting the X logical at any other yz slab boundary must be in the trivial equivalence class by Lemma 2. Hence the X logical within each yz slab can be multiplied by an X operator on each

boundary to create a logical operator supported within the slab. The resulting operator must be a stabilizer by the above lemma. Hence the X logical, multiplied by some X operators on the boundaries between slabs that create no excitations, is a product of stabilizers. The additional X operators between slabs are themselves stabilizers, which follows by considering them alone and shifting the boundaries of the yz slabs by a small amount, sufficient to bring the boundary operators wholly into single slabs. Hence the original X logical itself must be a product of stabilizers. \square

Remark 4. The above lemmas establish a one-to-one correspondence between logical X operators of the input code and logical operators of the related layer codes. Mapping from an input X logical to an X logical on a layer code can be achieved via the quasiconcatenated logical operators introduced in the previous section. Mapping from an X logical of the layer code to an X logical of the input code can be achieved by truncating the layer code X logical operator and mapping the configuration of m excitations it creates at the boundary of a yz slab to an input X logical.

Corollary 2. *The X distance of a family of layer codes based on an $[[n, k, d]]$ family of input codes satisfies $D_X = \Omega\left(\frac{1}{w}dn_Z\right)$. Here n_Z is the number of Z checks in the input code and w is the maximum check weight of the input code.*

Proof. The n_Z factor in the scaling of the logical X distance for the layer codes follows from the fact that nontrivial logical X operators must have support on all yz slabs. The $\frac{1}{w}d$ factor in the scaling of the logical X distance follows from the explanation in remark 2 that restricting any representative of a nontrivial logical X operator to a single yz slab results in a configuration of m excitations on each boundary of that slab with minimum weight $\frac{2}{w}d$. Moving $\frac{2}{w}d$ excitations into, and across, the slab from different points on the boundary requires an operator with weight $\Omega\left(\frac{2}{w}d\right)$. \square

B. Energy barrier for the Leverrier-Zemor codes

In this section we show that there exist good LDPC CSS codes with a linear energy barrier. For this purpose we focus on the Leverrier-Zemor (LZ) codes [35]. Since X and Z operators can be treated separately in CSS codes, we use the notation $y \in \{0, 1\}^n$ to specify an n -qubit X or Z operator depending on the context, $|\cdot|$ refers to the Hamming norm, and \oplus denotes binary addition. We write H_Z, H_X the Z and X parity check matrices. Similarly we write L_Z and L_X the non-trivial logical operators of the code. We state our argument explicitly for X logical operators,

and the Z case follows identically. We start by giving a formal definition to the strict version of the energy barrier described in Section II C.

Definition 3 (Energy barrier). *A code is said to have an energy barrier Δ if for any $y \in L_X$ and for any sequence $(y_i)_{i=1}^{i=l}$ of single-qubit operators such that $\bigoplus_{i=1}^{i=l} y_i = y$ there exists an index $e \leq l$ such that $|H_Z y'| \geq \Delta$, where $y' = \bigoplus_{i=1}^{i=e} y_i$, and similarly for L_Z, H_X .*

The LZ codes have the striking property that if y has a small syndrome then either it is very far from, or very close to, being a trivial operator. The notion of being “far” from the codespace is captured by the $|\cdot|_{S_X}$ (or $|\cdot|_{S_Z}$) norm:

$$|y|_{S_X} = \min_{s \in S_X} |y \oplus s|$$

and similarly for $|\cdot|_{S_Z}$.

It is easy to verify that for $\hat{x} \in \{0, 1\}^n$, with $|\hat{x}| \leq 1$, then

$$||y|_{S_X} - |y \oplus \hat{x}|_{S_X}| \leq 1,$$

which we refer to as the *continuity* of $|\cdot|_{S_X}$.

Lemma 5 ([35]). *For the codes defined in Ref. [35] there exist constants c_1, c_2, δ_0 such that for any $0 \leq \delta < \delta_0$, if $c_1 \delta n \leq |y|_{S_X} \leq c_2 n$, then $|H_Z y| > \delta n_Z$, where n_Z is the number of Z checks.*

Lemma 6. *The Leverrier-Zemor codes have an energy barrier scaling as $\Omega(n)$.*

Proof. Consider an arbitrary sequence $(y_i)_{i=1}^{i=l}$ of single-qubit operators such that $\bigoplus_{i=1}^{i=l} y_i = y$ for some non-trivial logical operator y . Note that by the definition of the distance, there exists an index e such that

$$\left| \bigoplus_{i=1}^{i=e} y_i \right|_{S_X} = \lfloor \min(c_2 n, d/2) \rfloor. \quad (18)$$

We will write $y' = \bigoplus_{i=1}^{i=e} y_i$. Given that $d \in \Omega(n)$, then there exists a constant $\delta' > 0$ independent of n such that $c_1 \delta' n < \lfloor \min(c_2 n, d/2) \rfloor$. That gives us

$$c_1 \delta' n \leq |y'|_{S_X} \leq c_2 n$$

This can be inserted into Lemma 5, and we verify that

$$|H_Z y'| \in \Omega(n)$$

□

VI. LATTICE MODEL

In order to build a physical model for the layer code construction in Section III, we need to specify explicit checks for each topological defect that appeared there. We note that these checks can be chosen so that the resulting layer code is CSS.

A. Layer checks

The stabilizer checks away from defects and boundaries are given by the canonical surface code checks, see Section II. The surface code layers have rough boundary conditions where they meet the xy boundary of the cuboid that bounds the layer code. Similarly, they have smooth boundary conditions where they meet the yz boundary of the cuboid, see Figure 16. This choice of boundary conditions is such that the \bar{X} logical operators are oriented along the \hat{x} direction and similarly \bar{Z} logical operators are oriented along \hat{z} , as depicted in Figure 5.

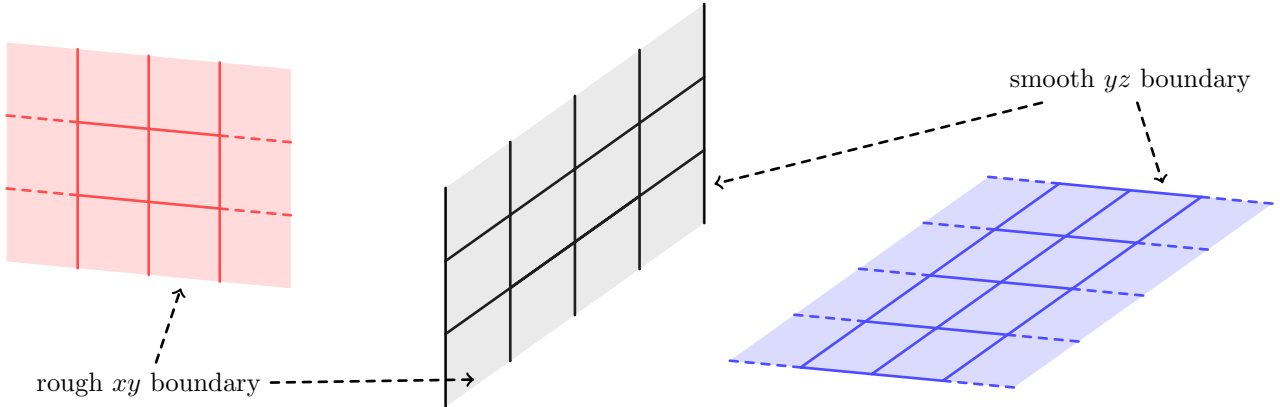
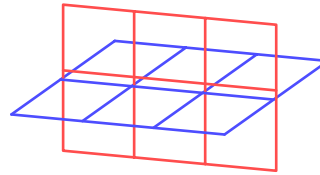


FIG. 16. A yz layer on the left with rough xy boundaries. An xz layer in the middle with both rough xy boundaries and smooth yz boundaries. An xy layer on the right with smooth yz boundaries.

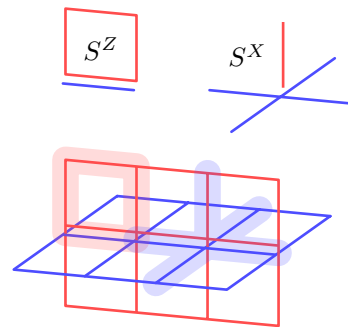
B. Line defect checks

We now turn to the implementation of the topological line defects. Below, we list only those checks that differ from the standard surface code stabilizers. There are 3 types of \hat{x} -oriented junctions, 2 types of \hat{y} -oriented junctions and 3 types of \hat{z} -oriented junctions.

1. The first, *trivial*, type of \hat{y} junction is simply a crossing an xy and a yz surface code layer with no coupling between the layers. The layers meet along a line of \hat{y} edges. The stabilizer checks for the two layers are separately given by canonical surface code terms.

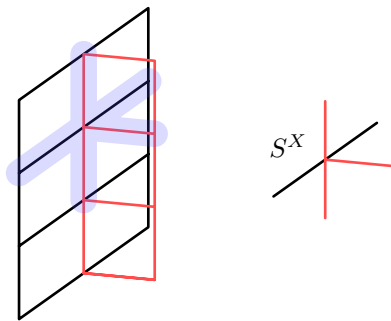


2. The second, *nontrivial*, type of \hat{y} junction has modified stabilizer checks that couple an xy and a yz surface code layer.

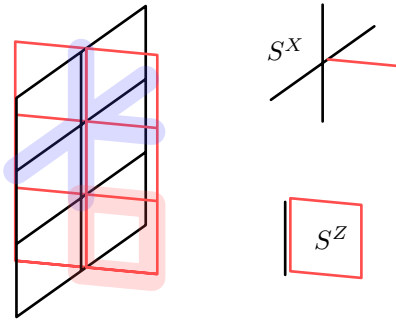


In this figure, and those below, the S^Z stabilizer on the region highlighted in red has support on the edges that are depicted adjacent to it. The S^X stabilizer on the region highlighted in blue is specified similarly.

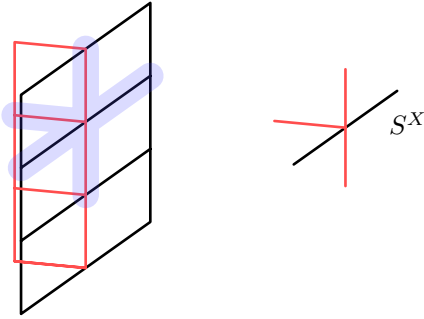
3. The *first* type of \hat{z} junction occurs where a yz layer meets its first xz layer. The star checks are modified along the junction.



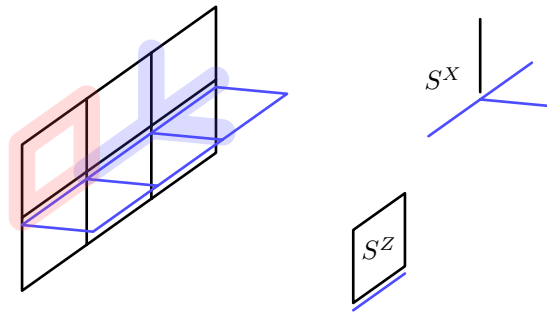
4. The second, *middle*, type of \hat{z} junction occurs where a yz layer intersects an xz layer. The star and plaquette checks are modified along the junction.



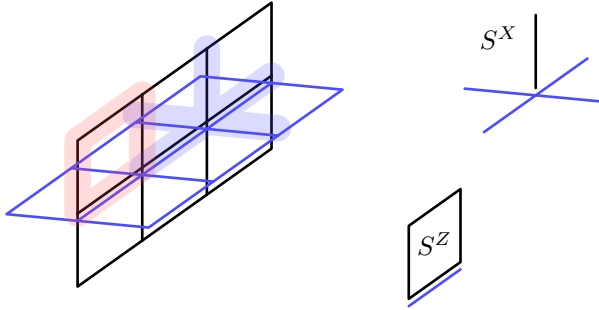
5. The third, *last*, type of \hat{z} junction occurs where a yz layer meets its last xz layer. It is simply a reflection of the first type of \hat{z} junction above.



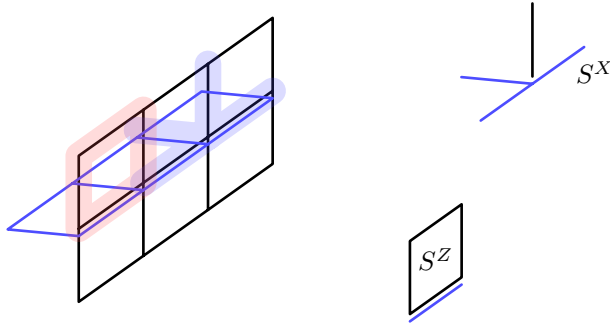
6. The *first* type of \hat{x} junction occurs where an xy layer meets its first xz layer. The star and plaquette checks are modified as follows along the junction.



7. The second, *middle*, type of \hat{x} junction occurs where an xy layer intersects an xz layer. The star and plaquette checks are modified along the junction.



8. The third, *last*, type of \hat{x} junction occurs where an xy layer meets its last xz layer.



This concludes the enumeration of line defect lattice checks.

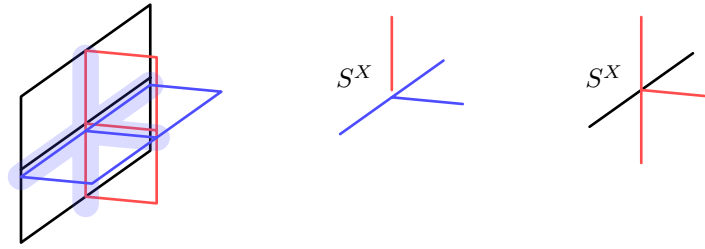
C. Point Defect Checks

In addition to the above line defects, there are 8 types of point defects in the bulk and 12 types of point defects on the boundary of the cuboid.

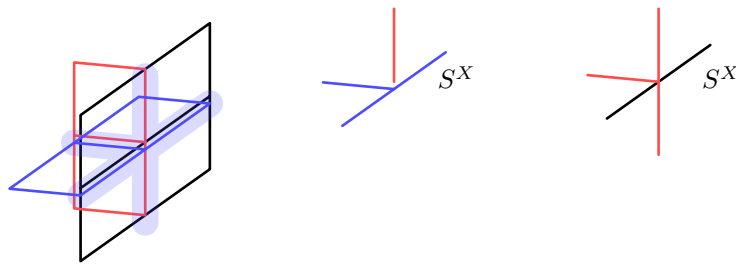
Bulk Point Defects

The 8 point defects in the bulk are listed below.

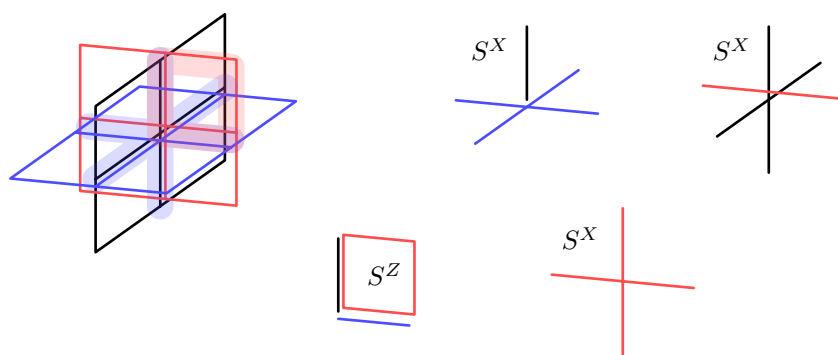
1. The first type of bulk point defect occurs at the intersection of a first \hat{x} junction, a first \hat{z} junction, and a nontrivial \hat{y} junction. The modified star checks at the point defect are shown directly below.



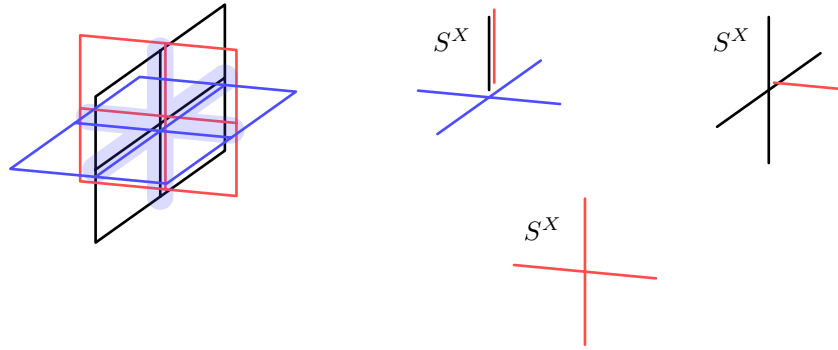
2. The second type of bulk point defect occurs at the intersection of a last \hat{x} junction, a last \hat{z} junction, and a nontrivial \hat{y} junction. This point defect is simply the reflection of the above through an xz plane. The modified star checks are shown directly below.



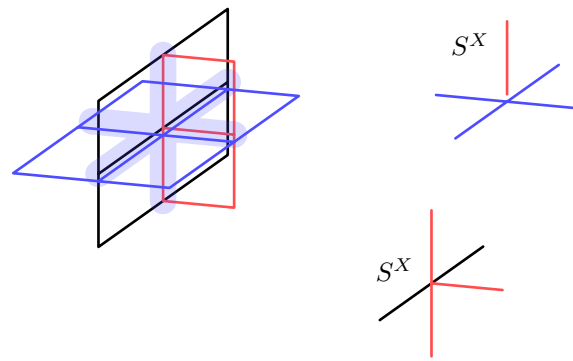
3. The third type of bulk point defect occurs at the intersection of a middle \hat{x} junction, a middle \hat{z} junction, a trivial \hat{y} junction from below and a nontrivial \hat{y} junction from above. The modified checks are shown directly below.



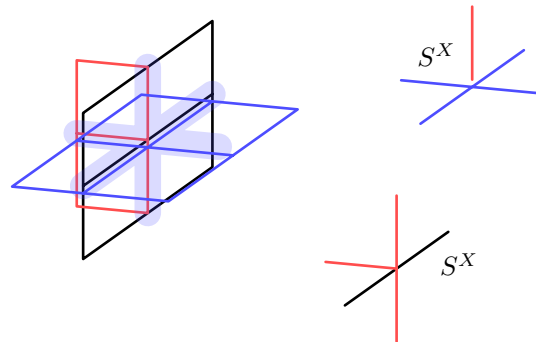
4. The fourth type of bulk point defect occurs at the intersection of a middle \hat{x} junction, a middle \hat{z} junction, a nontrivial \hat{y} junction from below and a trivial \hat{y} junction from above. This junction only differs from the above by the exchange of the trivial and nontrivial \hat{y} junctions. The modified checks are shown directly below.



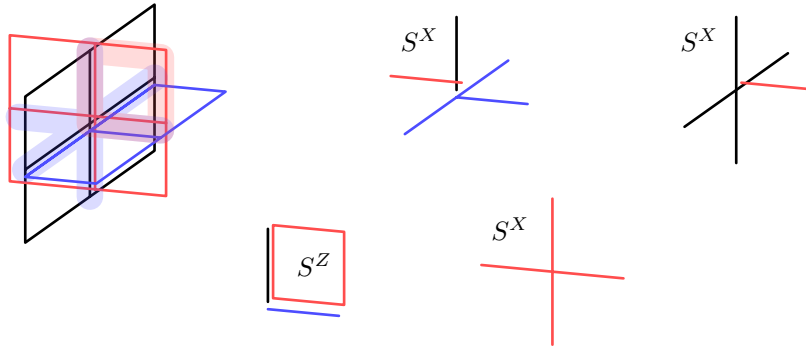
5. The fifth type of bulk point defect occurs at the intersection of a middle \hat{x} junction, a first \hat{z} junction, and a nontrivial \hat{y} junction from above. The modified star checks on the point defect are shown directly below.



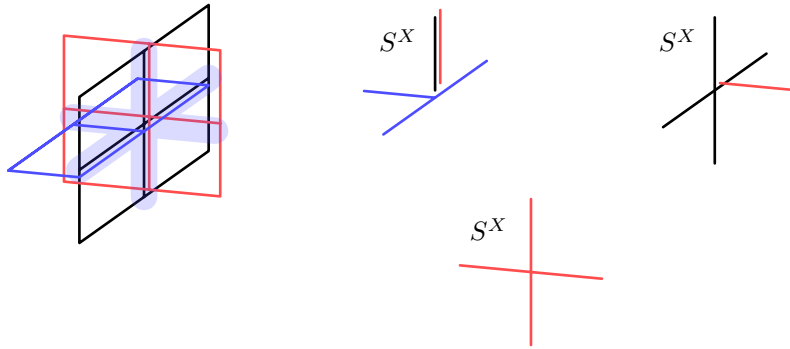
6. The sixth type of bulk point defect occurs at the intersection of a middle \hat{x} junction, a last \hat{z} junction, and a nontrivial \hat{y} junction from below. The modified star checks on the point defect are shown directly below.



7. The seventh type of bulk point defect occurs at the intersection of a first \hat{x} junction, a middle \hat{z} junction, and a nontrivial \hat{y} junction from above. The modified checks on the point defect are shown directly below.



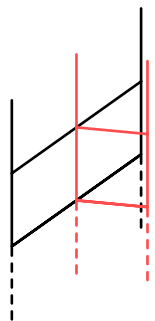
8. The seventh type of bulk point defect occurs at the intersection of a last \hat{x} junction, a middle \hat{z} junction, and a nontrivial \hat{y} junction from below. The modified checks on the point defect are shown directly below.



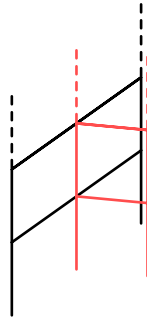
Boundary Point Defects

The 12 boundary point defects are listed below.

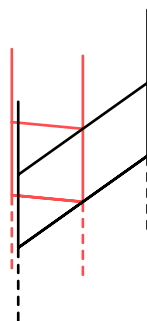
1. The first type of boundary point defect occurs where a first \hat{z} junction meets the front yz boundary. The stabilizer checks are given by standard surface code terms in the presence of a rough boundary and the trivalent junction introduced above.



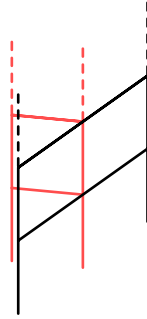
2. The second type of boundary point defect occurs where a first \hat{z} junction meets the back yz boundary. The stabilizer checks are given by standard surface code terms in the presence of a rough boundary and the trivalent junction introduced above. This is simply the reflection of the above point defect through a yz plane.



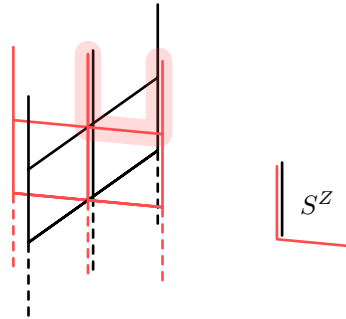
3. The third type of boundary point defect occurs where a last \hat{z} junction meets the front yz boundary. The stabilizer checks are given by standard surface code terms in the presence of a rough boundary and the trivalent junction introduced above. This is simply the reflection of the first boundary point defect through an xz plane.



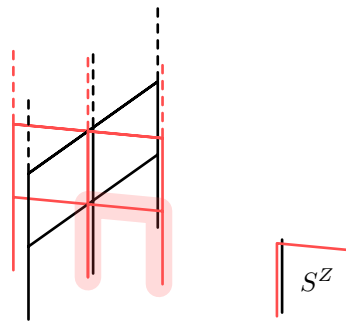
4. The fourth type of boundary point defect occurs where a last \hat{z} junction meets the back yz boundary. The stabilizer checks are given by standard surface code terms in the presence of a rough boundary and the trivalent junction introduced above. This is simply the reflection of the second boundary point defect through an xz plane.



5. The fifth type of boundary point defect occurs where a middle \hat{z} junction meets the front yz boundary. The stabilizer checks are given by standard surface code terms in the presence of a rough boundary and the middle \hat{z} junction introduced above, together with a modified plaquette term shown directly below.

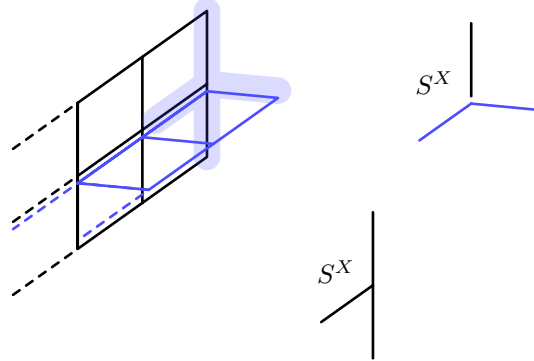


6. The sixth type of boundary point defect occurs where a middle \hat{z} junction meets the back yz boundary. This is given by the reflection of the fifth boundary point defect through an xy plane. The stabilizer checks are given by standard surface code terms in the presence of a rough boundary and the middle \hat{z} junction introduced above, together with a modified plaquette term shown directly below.

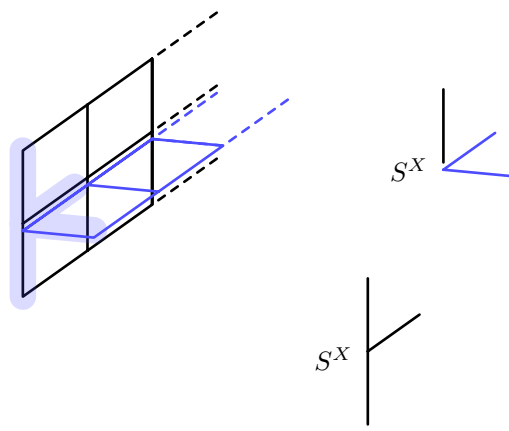


7. The seventh type of boundary point defect occurs where a first \hat{x} junction meets the left yz

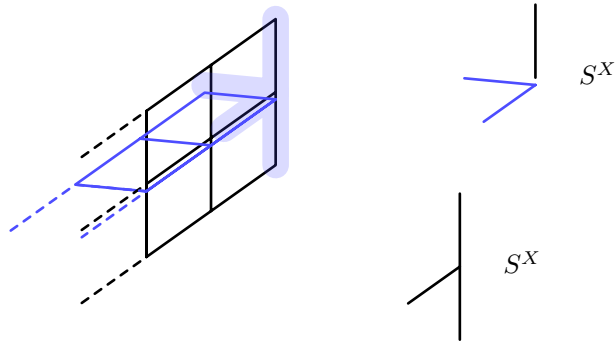
boundary. The stabilizer checks are given by standard surface code terms with a smooth boundary and the \hat{x} junction introduced above, together with modified boundary star checks.



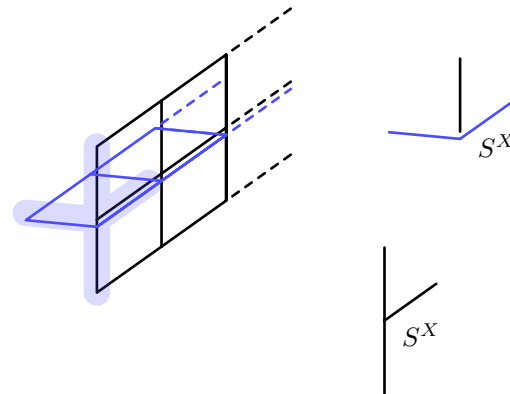
8. The eighth type of boundary point defect occurs where a first \hat{x} junction meets the right yz boundary. This is simply the reflection of the above point defect through the yz plane. The stabilizer checks are given by standard surface code terms with a smooth boundary and the \hat{x} junction introduced above, together with modified boundary star checks shown directly below.



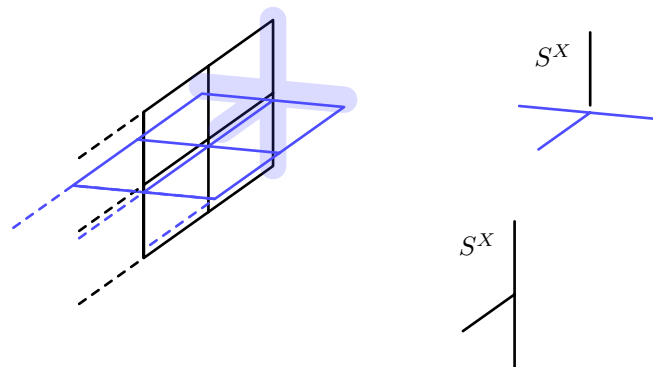
9. The ninth type of boundary point defect occurs where a last \hat{x} junction meets the left yz boundary. The stabilizer checks are given by standard surface code terms with a smooth boundary and the \hat{x} junction introduced above, together with modified boundary star checks shown directly below.



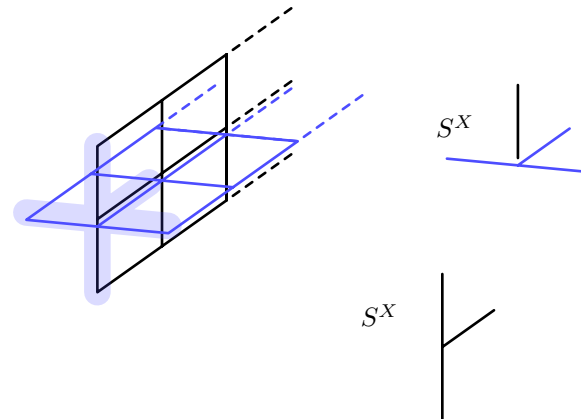
10. The tenth type of boundary point defect occurs where a last \hat{x} junction meets the right yz boundary. This is given by reflecting the above point defect through the yz plane. The stabilizer checks are given by standard surface code terms with a smooth boundary and the \hat{x} junction introduced above, together with modified boundary star checks shown directly below.



11. The eleventh type of boundary point defect occurs where a middle \hat{x} junction meets the left yz boundary. The stabilizer checks are given by standard surface code terms with a smooth boundary and the middle \hat{x} junction introduced above, together with modified boundary star checks shown directly below.



12. The twelfth type of boundary point defect occurs where a middle \hat{x} junction meets the right yz boundary. This is given by reflecting the above point defect through a yz plane. The stabilizer checks are given by standard surface code terms with a smooth boundary and the middle \hat{x} junction introduced above, together with modified boundary star checks shown directly below.



This concludes the enumeration of point defect lattice checks.

VII. DISCUSSION

In this work we introduced a construction that takes as input an arbitrary $[[n, k, d]]$ CSS stabilizer code and produces as output a layer code, which is a $[[\Theta(nn_Xn_Z), k, \Omega(\frac{1}{w}dn)]]$ CSS stabilizer code that is local in three dimensional space. Here n_X denotes the number of X checks, n_Z the number of Z checks, and w the maximum weight of the checks in the input code. Each layer code has checks of weight 6 or less, and takes the form of a topological defect network. The name layer code reflects that these codes are a special variety of topological defect network that is built exclusively from layers of surface code, one for each physical qubit and stabilizer check of the input code, joined together by line defects with incidence relations inherited from the Tanner graph of the input code.

Applying our construction to a family of good quantum LDPC CSS codes with parameters $[[n, \Theta(n), \Theta(n)]]$ produces a family of layer codes with parameters $[[\Theta(n^3), \Theta(n), \Theta(n^2)]]$, which is optimal for a family of three dimensional topological codes. While our construction applies to general input CSS codes that are not necessarily LDPC, we can only guarantee favorable scaling of the output code's distance when the maximum stabilizer weight of the input code is constant.

We have shown that the layer codes output by our construction preserve the scaling of the energy barrier of an input LDPC code. Hence any layer code family that is based on a family of input codes with a polynomial energy barrier also has a polynomial energy barrier. We proved that the LDPC codes introduced in Ref. [35] have a linear energy barrier $\Theta(n)$, where n is the number of physical qubits. Hence there exist layer codes with $\Theta(n^3)$ physical qubits and energy barrier $\Theta(n)$. This raises the question of whether any layer code family with optimal code parameters and polynomial energy barrier is a self-correcting quantum memory. We leave this question to future work.

We remark that our construction depends on the choice of stabilizer generators, or checks, of the input code. This raises the question of how the output codes produced from the same input code with different choices of generators are related. In particular, are output codes with different choices of input generators in the same topological phase of matter? That is, are they equivalent up to a generalized local unitary in three dimensions? Similarly, we have not addressed the question of how the layer code output by our construction is related to the three dimensional code output by the construction of Ref. [89] for the same input LDPC code.

We have not addressed the important problem of decoding layer codes in this work. We remark that the general renormalization group decoder [63] is applicable to layer codes, as they satisfy the local topological order condition in three dimensions. However, the structure of the layer codes suggests that more specialized decoders should exist. We have also not addressed the problem of performing fault-tolerant logical gates on the layer codes. The surface code layer structure of the layer codes presents a great opportunity to leverage well-developed surface code techniques for performing such gates. We leave these directions to future work.

Several extensions of this work present themselves. First, it would be interesting to find a floquet implementation of the layer codes that reduces the check weight to 2. It would also be interesting to extend our construction to color code layers via folding [113] in a way that preserves the transversal gates of the input code, such as the Steane code example. Another question is about the generalization of our construction to non-CSS codes, and codes beyond the Pauli stabilizer formalism. Can our construction be leveraged to build translation invariant topological codes in three dimensions with optimal code parameters?

An interesting challenge is the extension of our construction to higher dimensions in a way that produces output codes that saturate the BPT bound in all dimensions. Similarly, it would be interesting to generalize our construction to produce optimal codes in spaces with constant negative curvature, rather than flat space. It would also be interesting to generalize the construction of layer

codes to allow arbitrary nonlocal, but low weight, connections between the surface codes and to explore the tradeoff in code parameters and properties that this allows. This could open a path to apply extremely well developed surface code techniques to good LDPC codes.

- [1] R. P. Feynman, Simulating physics with computers, *International Journal of Theoretical Physics* **21**, [10.1007/BF02650179](https://doi.org/10.1007/BF02650179) (1982).
- [2] Y. Manin, Computable and uncomputable, *Sovetskoye Radio, Moscow* **128**, 28 (1980).
- [3] P. Benioff, The computer as a physical system: A microscopic quantum mechanical Hamiltonian model of computers as represented by Turing machines, *Journal of Statistical Physics* **22**, [10.1007/BF01011339](https://doi.org/10.1007/BF01011339) (1980).
- [4] D. Deutsch, QUANTUM THEORY, THE CHURCH-TURING PRINCIPLE AND THE UNIVERSAL QUANTUM COMPUTER., *Proceedings of The Royal Society of London, Series A: Mathematical and Physical Sciences* **400**, [10.1098/rspa.1985.0070](https://doi.org/10.1098/rspa.1985.0070) (1985).
- [5] G. Q. AI and Collaborators, Quantum supremacy using a programmable superconducting processor, *Nature* **574**, [10.1038/s41586-019-1666-5](https://doi.org/10.1038/s41586-019-1666-5) (2019).
- [6] P. W. Shor, Scheme for reducing decoherence in quantum computer memory, *Physical Review A* **52**, R2493 (1995).
- [7] A. M. Steane, Error correcting codes in quantum theory, *Physical Review Letters* **77**, [10.1103/PhysRevLett.77.793](https://doi.org/10.1103/PhysRevLett.77.793) (1996).
- [8] P. W. Shor, Fault-tolerant quantum computation, in *Proceedings of 37th Conference on Foundations of Computer Science* (IEEE, 1996) pp. 56–65.
- [9] D. Gottesman, Stabilizer codes and quantum error correction, arXiv preprint [quant-ph/9705052](https://arxiv.org/abs/quant-ph/9705052) (1997).
- [10] D. Aharonov and M. Ben-Or, Fault-tolerant quantum computation with constant error, in *Proceedings of the twenty-ninth annual ACM symposium on Theory of computing* (ACM, 1997) pp. 176–188.
- [11] E. Knill, R. Laflamme, and W. H. Zurek, Resilient quantum computation, *Science* **279**, 342 (1998).
- [12] A. Y. Kitaev, Quantum computations: algorithms and error correction, *Russian Mathematical Surveys* **52**, 1191 (1997).
- [13] J. Preskill, Reliable quantum computers, *Proceedings of the Royal Society A: Mathematical, Physical and Engineering Sciences* **454**, 385 (1998), arXiv:9705031 [quant-ph].
- [14] J. Preskill, Fault-tolerant quantum computation, in *Proceedings of 37th Conference on Foundations of Computer Science* (WORLD SCIENTIFIC, 1997) pp. 56–65, arXiv:9712048 [quant-ph].
- [15] A. Y. Kitaev, Fault-tolerant quantum computation by anyons, *Annals of Physics* **303**, 2 (2003).
- [16] S. Bravyi and A. Y. Kitaev, Quantum codes on a lattice with boundary, arXiv preprint [quant-ph/9811052](https://arxiv.org/abs/quant-ph/9811052) (1998).

- [17] E. Dennis, A. Kitaev, A. Landahl, and J. Preskill, Topological quantum memory, *Journal of Mathematical Physics* **43**, 4452 (2002).
- [18] R. Raussendorf and J. Harrington, Fault-tolerant quantum computation with high threshold in two dimensions, *Physical Review Letters* **98**, 190504 (2007).
- [19] R. Raussendorf, J. Harrington, and K. Goyal, Topological fault-tolerance in cluster state quantum computation, *New Journal of Physics* **9**, 199 (2007).
- [20] L. Postler, S. Heußen, I. Pogorelov, M. Rispler, T. Feldker, M. Meth, C. D. Marciak, R. Stricker, M. Ringbauer, R. Blatt, P. Schindler, M. Müller, and T. Monz, Demonstration of fault-tolerant universal quantum gate operations, *Nature* **605**, [10.1038/s41586-022-04721-1](https://doi.org/10.1038/s41586-022-04721-1) (2022).
- [21] S. Krinner, N. Lacroix, A. Remm, A. Di Paolo, E. Genois, C. Leroux, C. Hellings, S. Lazar, F. Swiadek, J. Herrmann, G. J. Norris, C. K. Andersen, M. Müller, A. Blais, C. Eichler, and A. Wallraff, Realizing repeated quantum error correction in a distance-three surface code, *Nature* **605**, [10.1038/s41586-022-04566-8](https://doi.org/10.1038/s41586-022-04566-8) (2022).
- [22] G. Q. Ai, Suppressing quantum errors by scaling a surface code logical qubit, *Nature* **614**, [10.1038/s41586-022-05434-1](https://doi.org/10.1038/s41586-022-05434-1) (2023).
- [23] D. Gottesman, Fault-tolerant quantum computation with constant overhead, *Quantum Information & Computation* **14**, 1338 (2014).
- [24] J.-P. Tillich and G. Zémor, Quantum LDPC codes with positive rate and minimum distance proportional to the square root of the blocklength, *IEEE Transactions on Information Theory* **60**, 1193 (2014).
- [25] A. Leverrier, J.-P. Tillich, and G. Zémor, Quantum expander codes, in *Foundations of Computer Science (FOCS), 2015 IEEE 56th Annual Symposium on* (IEEE, 2015) pp. 810–824.
- [26] N. P. Breuckmann and J. Eberhardt, LDPC quantum codes, arXiv preprint arXiv:2103.06309 (2021).
- [27] F. J. Wegner, Duality in generalized Ising models and phase transitions without local order parameters, *Journal of Mathematical Physics* **12**, [10.1063/1.1665530](https://doi.org/10.1063/1.1665530) (1971).
- [28] J. B. Kogut, An introduction to lattice gauge theory and spin systems, *Reviews of Modern Physics* **51**, 659 (1979).
- [29] R. Dijkgraaf and E. Witten, Topological gauge theories and group cohomology, *Communications in Mathematical Physics* **129**, 393 (1990).
- [30] A. Kitaev, Anyons in an exactly solved model and beyond, *Annals of Physics* **321**, 2 (2006), [arXiv:0506438 \[cond-mat\]](https://arxiv.org/abs/0506438).
- [31] M. B. Hastings, J. Haah, and R. O'Donnell, Fiber bundle codes: Breaking the $N^{1/2}\text{polylog}(N)$ barrier for quantum LDPC codes, arXiv preprint arXiv:2009.03921 (2020).
- [32] P. Panteleev and G. Kalachev, Quantum LDPC codes with almost linear minimum distance, arXiv preprint arXiv:2012.04068 (2020).
- [33] N. P. Breuckmann and J. N. Eberhardt, Balanced product quantum codes, arXiv preprint arXiv:2012.09271 (2020).

- [34] Asymptotically good Quantum and locally testable classical LDPC codes, in *Proceedings of the Annual ACM Symposium on Theory of Computing* (2022).
- [35] A. Leverrier and G. Zémor, *Quantum tanner codes* (2022).
- [36] I. Dinur, M. H. Hsieh, T. C. Lin, and T. Vidick, Good Quantum LDPC Codes with Linear Time Decoders, in *Proceedings of the Annual ACM Symposium on Theory of Computing* (2023).
- [37] S. Bravyi, D. Poulin, and B. Terhal, Tradeoffs for reliable quantum information storage in 2D systems, *Physical Review Letters* **104**, 050503 (2010).
- [38] S. Bravyi and B. Terhal, A no-go theorem for a two-dimensional self-correcting quantum memory based on stabilizer codes, *New Journal of Physics* **11**, 043029 (2009).
- [39] J. Haah, A degeneracy bound for homogeneous topological order, *SciPost Physics* **10**, [10.21468/SciPostPhys.10.1.011](https://doi.org/10.21468/SciPostPhys.10.1.011) (2021).
- [40] A. R. Calderbank and P. W. Shor, Good quantum error-correcting codes exist, *Physical Review A* **54**, 1098 (1996).
- [41] A. M. Steane, Simple quantum error-correcting codes, *Physical Review A - Atomic, Molecular, and Optical Physics* **54**, 4741 (1996), [arXiv:9605021](https://arxiv.org/abs/9605021) [quant-ph].
- [42] K. Slagle, D. Aasen, and D. Williamson, Foliated field theory and string-membrane-net condensation picture of fracton order, *SciPost Physics* **6**, [10.21468/scipostphys.6.4.043](https://doi.org/10.21468/scipostphys.6.4.043) (2019), [arXiv:1812.01613](https://arxiv.org/abs/1812.01613).
- [43] D. Aasen, D. Bulmash, A. Prem, K. Slagle, and D. J. Williamson, Topological defect networks for fractons of all types, *Physical Review Research* **2**, [10.1103/physrevresearch.2.043165](https://doi.org/10.1103/physrevresearch.2.043165) (2020), [arXiv:2002.05166](https://arxiv.org/abs/2002.05166).
- [44] Z. Song, A. Dua, W. Shirley, and D. J. Williamson, Topological defect network representations of fracton stabilizer codes [10.48550/arxiv.2112.14717](https://doi.org/10.48550/arxiv.2112.14717) (2021), [arXiv:2112.14717](https://arxiv.org/abs/2112.14717).
- [45] H. Bombin and M. A. Martin-Delgado, Exact topological quantum order in $D = 3$ and beyond: Branyons and brane-net condensates, *Physical Review B* **75**, 075103 (2007).
- [46] H. Bombín, Gauge color codes: Optimal transversal gates and gauge fixing in topological stabilizer codes, *New Journal of Physics* **17**, [10.1088/1367-2630/17/8/083002](https://doi.org/10.1088/1367-2630/17/8/083002) (2015), [arXiv:1311.0879](https://arxiv.org/abs/1311.0879).
- [47] B. J. Brown, D. Loss, J. K. Pachos, C. N. Self, and J. R. Wootton, Quantum memories at finite temperature, *Reviews of Modern Physics* **88**, [10.1103/revmodphys.88.045005](https://doi.org/10.1103/revmodphys.88.045005) (2016).
- [48] C. Castelnovo and C. Chamon, Entanglement and topological entropy of the toric code at finite temperature, *Physical Review B - Condensed Matter and Materials Physics* **76**, [10.1103/PhysRevB.76.184442](https://doi.org/10.1103/PhysRevB.76.184442) (2007), [arXiv:0704.3616](https://arxiv.org/abs/0704.3616).
- [49] C. Castelnovo and C. Chamon, Topological order in a three-dimensional toric code at finite temperature, *Physical Review B - Condensed Matter and Materials Physics* **78**, [10.1103/PhysRevB.78.155120](https://doi.org/10.1103/PhysRevB.78.155120) (2008), [arXiv:0804.3591](https://arxiv.org/abs/0804.3591).
- [50] B. Yoshida, Classification of quantum phases and topology of logical operators in an exactly solved model of quantum codes, *Annals of Physics* **326**, 15 (2011), [arXiv:1007.4601](https://arxiv.org/abs/1007.4601).
- [51] B. Yoshida, Feasibility of self-correcting quantum memory and thermal stability of topological order,

Annals of Physics **326**, 10.1016/j.aop.2011.06.001 (2011).

[52] C. Chamon, Quantum glassiness in strongly correlated clean systems: An example of topological overprotection, *Physical Review Letters* **94**, 40402 (2005), arXiv:0404182 [cond-mat].

[53] J. Haah, Local stabilizer codes in three dimensions without string logical operators, *Physical Review A* **83**, 10.1103/physreva.83.042330 (2011).

[54] K. Walker and Z. Wang, (3+1)-TQFTs and topological insulators, *Frontiers of Physics* **7**, 150 (2012), arXiv:1104.2632.

[55] I. H. Kim, 3D local qudit quantum code without string logical operator, arXiv , 9 (2012), arXiv:1202.0052.

[56] B. Yoshida, Exotic topological order in fractal spin liquids, *Physical Review B - Condensed Matter and Materials Physics* **88**, 125122 (2013), arXiv:1302.6248.

[57] S. Vijay, J. Haah, and L. Fu, A new kind of topological quantum order: A dimensional hierarchy of quasiparticles built from stationary excitations, *Physical Review B - Condensed Matter and Materials Physics* **92**, 235136 (2015), arXiv:1505.02576.

[58] S. Vijay, J. Haah, and L. Fu, Fracton Topological Order, Generalized Lattice Gauge Theory and Duality, *Physical Review B* **10.1103/physrevb.94.235157** (2016), arXiv:1603.04442.

[59] D. J. Williamson, Fractal symmetries: Ungauging the cubic code, *Physical Review B* **94**, 10.1103/physrevb.94.155128 (2016), arXiv:1603.05182.

[60] S. Bravyi, B. Leemhuis, and B. M. Terhal, Topological order in an exactly solvable 3D spin model, *Ann. Phys.* **326**, 839 (2010), arXiv:1006.4871.

[61] K. Michnicki, 3-d quantum stabilizer codes with a power law energy barrier (2012).

[62] S. Bravyi and J. Haah, Energy landscape of 3D spin hamiltonians with topological order, *Physical Review Letters* **107**, 150504 (2011), arXiv:1105.4159.

[63] S. Bravyi and J. Haah, Quantum self-correction in the 3d cubic code model, *Physical Review Letters* **111**, 10.1103/physrevlett.111.200501 (2013).

[64] D. J. Williamson and Z. Wang, Hamiltonian models for topological phases of matter in three spatial dimensions, *Annals of Physics* **377**, 311 (2017), arXiv:1606.07144.

[65] B. J. Brown and D. J. Williamson, Parallelized quantum error correction with fracton topological codes, *Physical Review Research* **2**, 1 (2020), arXiv:1901.08061.

[66] Z. Weinstein, G. Ortiz, and Z. Nussinov, Universality Classes of Stabilizer Code Hamiltonians, *Physical Review Letters* **123**, 10.1103/PhysRevLett.123.230503 (2019).

[67] T. Devakul and D. J. Williamson, Fractalizing quantum codes, *Quantum* **5**, 10.22331/q-2021-04-22-438 (2021), arXiv:2009.01252.

[68] G. Zhu, T. Jochym-O'Connor, and A. Dua, Topological Order, Quantum Codes, and Quantum Computation on Fractal Geometries, *PRX Quantum* **3**, 10.1103/PRXQuantum.3.030338 (2022).

[69] C. T. Aitchison, D. Bulmash, A. Dua, A. C. Doherty, and D. J. Williamson, No strings attached: Boundaries and defects in the cubic code, arXiv preprint arXiv:2308.00138 (2023).

- [70] J. Haah, Bifurcation in entanglement renormalization group flow of a gapped spin model, *Physical Review B - Condensed Matter and Materials Physics* **89**, 75119 (2014), [arXiv:1310.4507](https://arxiv.org/abs/1310.4507).
- [71] S. Vijay and L. Fu, A Generalization of Non-Abelian Anyons in Three Dimensions, (2017), [arXiv:1706.07070](https://arxiv.org/abs/1706.07070).
- [72] H. Ma, E. Lake, X. Chen, and M. Hermele, Fracton topological order via coupled layers, *Physical Review B* **95**, 245126 (2017), [arXiv:1701.00747](https://arxiv.org/abs/1701.00747).
- [73] A. Dua, I. H. Kim, M. Cheng, and D. J. Williamson, Sorting topological stabilizer models in three dimensions, *Physical Review B* **100**, 10.1103/PhysRevB.100.155137 (2019), [arXiv:1908.08049](https://arxiv.org/abs/1908.08049).
- [74] A. Dua, D. J. Williamson, J. Haah, and M. Cheng, Compactifying fracton stabilizer models, *Physical Review B* **99**, 10.1103/physrevb.99.245135 (2019), [arXiv:1903.12246](https://arxiv.org/abs/1903.12246).
- [75] S. Pai and M. Hermele, Fracton fusion and statistics, *Physical Review B* **100**, 10.1103/PhysRevB.100.195136 (2019), [arXiv:1903.11625](https://arxiv.org/abs/1903.11625).
- [76] N. Tantivasadakarn and S. Vijay, Searching for Fracton Orders via Symmetry Defect Condensation, (2019), [arXiv:1912.02826](https://arxiv.org/abs/1912.02826).
- [77] N. Tantivasadakarn, W. Ji, and S. Vijay, Hybrid fracton phases: Parent orders for liquid and nonliquid quantum phases, *Physical Review B* **103**, 10.1103/PhysRevB.103.245136 (2021), [arXiv:2102.09555](https://arxiv.org/abs/2102.09555).
- [78] N. Tantivasadakarn, W. Ji, and S. Vijay, Non-Abelian hybrid fracton orders, *Physical Review B* **104**, 10.1103/PhysRevB.104.115117 (2021), [arXiv:2106.03842](https://arxiv.org/abs/2106.03842).
- [79] H. Song, N. Tantivasadakarn, W. Shirley, and M. Hermele, Fracton Self-Statistics, (2023), [arXiv:2304.00028](https://arxiv.org/abs/2304.00028).
- [80] D. Bulmash and T. Iadecola, Braiding and gapped boundaries in fracton topological phases, *Physical Review B* **99**, 10.1103/PhysRevB.99.125132 (2019), [arXiv:1810.00012](https://arxiv.org/abs/1810.00012).
- [81] H. Song, A. Prem, S. J. Huang, and M. A. Martin-Delgado, Twisted fracton models in three dimensions, *Physical Review B* **99**, 10.1103/PhysRevB.99.155118 (2019), [arXiv:1805.06899](https://arxiv.org/abs/1805.06899).
- [82] A. Prem and D. Williamson, Gauging permutation symmetries as a route to non-Abelian fractons, *SciPost Physics* **7**, 068 (2019), [arXiv:1905.06309](https://arxiv.org/abs/1905.06309).
- [83] A. Prem, S. J. Huang, H. Song, and M. Hermele, Cage-Net Fracton Models, *Physical Review X* **9**, 10.1103/PhysRevX.9.021010 (2019), [arXiv:1806.04687](https://arxiv.org/abs/1806.04687).
- [84] D. Bulmash and M. Barkeshli, Gauging fractons: Immobile non-Abelian quasiparticles, fractals, and position-dependent degeneracies, *Physical Review B* **100**, 10.1103/PhysRevB.100.155146 (2019), [arXiv:1905.05771](https://arxiv.org/abs/1905.05771).
- [85] A. Dua, P. Sarkar, D. J. Williamson, and M. Cheng, Bifurcating entanglement-renormalization group flows of fracton stabilizer models, *PHYSICAL REVIEW RESEARCH* **2**, 33021 (2019), [arXiv:1909.12304](https://arxiv.org/abs/1909.12304).
- [86] D. J. Williamson and M. Cheng, Designer non-Abelian fractons from topological layers, *Physical Review B* **107**, 10.1103/PhysRevB.107.035103 (2023), [arXiv:2004.07251](https://arxiv.org/abs/2004.07251).
- [87] J. Sullivan, T. Iadecola, and D. J. Williamson, Planar p-string condensation: Chiral fracton

phases from fractional quantum Hall layers and beyond, *Physical Review B* **103**, [10.1103/PhysRevB.103.205301](https://doi.org/10.1103/PhysRevB.103.205301) (2021), [arXiv:2010.15127](https://arxiv.org/abs/2010.15127).

[88] D. J. Williamson, Saturating tradeoff bounds with topological defect networks, talk at YITP workshop “Quantum Error Correction” <https://www.yukawa.kyoto-u.ac.jp/seminar/s53088> (2023).

[89] E. Portnoy, *Local quantum codes from subdivided manifolds* (2023).

[90] M. Freedman and M. Hastings, Building manifolds from quantum codes, *Geometric and Functional Analysis* **31**, [10.1007/s00039-021-00567-3](https://doi.org/10.1007/s00039-021-00567-3) (2021).

[91] M. Gromov and L. Guth, Generalizations of the Kolmogorov-Barzlin embedding estimates, *Duke Mathematical Journal* **161**, [10.1215/00127094-1812840](https://doi.org/10.1215/00127094-1812840) (2012).

[92] A. Steane, Multiple-particle interference and quantum error correction, *Proceedings of the Royal Society A* **452**, 2551 (1996).

[93] B. Zeng, X. Chen, D.-l. Zhou, and X.-G. Wen, *Quantum Information Meets Quantum Matter*, Quantum Science and Technology No. August (Springer New York, New York, NY, 2015) [arXiv:1508.02595](https://arxiv.org/abs/1508.02595).

[94] S. Bravyi, M. B. Hastings, and S. Michalakis, Topological quantum order: Stability under local perturbations, *Journal of Mathematical Physics* **51**, [10.1063/1.3490195](https://doi.org/10.1063/1.3490195) (2010).

[95] E. Knill and R. Laflamme, Theory of quantum error-correcting codes, *Phys. Rev. A* **55**, 900 (1997).

[96] M. Levin and X. G. Wen, Fermions, strings, and gauge fields in lattice spin models, *Physical Review B - Condensed Matter and Materials Physics* **67**, [10.1103/PhysRevB.67.245316](https://doi.org/10.1103/PhysRevB.67.245316) (2003).

[97] T. D. Ellison, Y. A. Chen, A. Dua, W. Shirley, N. Tantivasadakarn, and D. J. Williamson, Pauli Stabilizer Models of Twisted Quantum Doubles, *PRX Quantum* **3**, [10.1103/PRXQuantum.3.010353](https://doi.org/10.1103/PRXQuantum.3.010353) (2022).

[98] G. Moore and N. Seiberg, Classical and quantum conformal field theory, *Communications in Mathematical Physics* **123**, 177 (1989).

[99] S. Beigi, P. W. Shor, and D. Whalen, The Quantum Double Model with Boundary: Condensations and Symmetries, *Communications in Mathematical Physics* **306**, 663 (2011), [arXiv:1006.5479](https://arxiv.org/abs/1006.5479).

[100] A. Kitaev and L. Kong, Models for Gapped Boundaries and Domain Walls, *Communications in Mathematical Physics* **313**, 351 (2012), [arXiv:1104.5047](https://arxiv.org/abs/1104.5047).

[101] F. A. Bais and J. K. Slingerland, Condensate-induced transitions between topologically ordered phases, *Physical Review B - Condensed Matter and Materials Physics* **79**, [10.1103/PhysRevB.79.045316](https://doi.org/10.1103/PhysRevB.79.045316) (2009), [arXiv:0808.0627](https://arxiv.org/abs/0808.0627).

[102] M. Levin, Protected Edge Modes without Symmetry, *Physical Review X* **3**, [10.1103/PhysRevX.3.021009](https://doi.org/10.1103/PhysRevX.3.021009) (2013), [arXiv:1301.7355](https://arxiv.org/abs/1301.7355).

[103] L. Kong, Anyon condensation and tensor categories, *Nuclear Physics B* **886**, 436 (2014), [arXiv:1307.8244](https://arxiv.org/abs/1307.8244).

[104] D. Aasen, E. Lake, and K. Walker, Fermion condensation and super pivotal categories, *Journal of Mathematical Physics* **60**, [10.1063/1.5045669](https://doi.org/10.1063/1.5045669) (2019), [arXiv:1709.01941](https://arxiv.org/abs/1709.01941).

[105] H. Bombin, Topological order with a twist: Ising anyons from an abelian model, *Physical Review*

Letters **105**, 030403 (2010).

[106] J. Haah, An Invariant of Topologically Ordered States Under Local Unitary Transformations, *Communications in Mathematical Physics* **342**, 771 (2016), [arXiv:1407.2926](https://arxiv.org/abs/1407.2926).

[107] C. Horsman, A. G. Fowler, S. Devitt, and R. Van Meter, Surface code quantum computing by lattice surgery, *New Journal of Physics* **14**, 123011 (2012).

[108] E. Witten, Topological quantum field theory, *Communications in Mathematical Physics* **1988** **117**:3 **117**, 353 (1988).

[109] M. Atiyah, Topological quantum field theories, *Publications Mathématiques de l’Institut des Hautes Scientifiques* **68**, 175 (1988), [arXiv:0011260 \[hep-th\]](https://arxiv.org/abs/0011260).

[110] T. D. Ellison, Y.-A. Chen, A. Dua, W. Shirley, N. Tantivasadakarn, and D. J. Williamson, Pauli topological subsystem codes from abelian anyon theories, arXiv preprint [arXiv:2211.03798](https://arxiv.org/abs/2211.03798) (2022).

[111] M. S. Kesselring, J. C. M. de la Fuente, F. Thomsen, J. Eisert, S. D. Bartlett, and B. J. Brown, Anyon condensation and the color code, arXiv preprint [arXiv:2212.00042](https://arxiv.org/abs/2212.00042) (2022).

[112] B. J. Brown, Conservation Laws and Quantum Error Correction: Towards a Generalised Matching Decoder, *IEEE BITS the Information Theory Magazine* [10.1109/mbits.2023.3246025](https://doi.org/10.1109/mbits.2023.3246025) (2023).

[113] A. Kubica, B. Yoshida, and F. Pastawski, Unfolding the color code, *New Journal of Physics* **17**, 83026 (2015), [arXiv:1503.02065](https://arxiv.org/abs/1503.02065).